SENSING PLATFORM AND OBJECT MOTION DETECTION BASED ON PASSIVE UHF RFID TAGS USING A HIDDEN MARKOV MODEL-BASED CLASSIFIER

by

YOUNG HO LEE

A dissertation submitted to the
Graduate School – New Brunswick
Rutgers, The State University of New Jersey
In partial fulfillment of the requirements
For the degree of
Doctor of Philosophy
Graduate Program in Electrical and Computer Engineering
Written under the direction of
Ivan Marsic
And approved by

_____

_____

_____

_____

New Brunswick, New Jersey
OCTOBER, 2017

ABSTRACT OF THE DESSERTATION

Sensing Platform and Object Motion Detection Based on Passive UHF RFID Tags Using a Hidden Markov Model –Based Classifier

by YOUNG HO LEE

Dissertation Director:

IVAN MARSIC

For context-aware systems in indoor work settings, several types of sensors have been applied to capture work activities. We introduce and present a sensing platform and object motion detection system using a hidden Markov Classifier based on a UHF RFID system. Backscattered signal strength of passive UHF RFID tags as a sensor is used for providing information on the movement and identity of work objects. As the read range of passive UHF RFID broadens up to 12 meters compared to 1-meter range of HF RFID, passive tags have been used for many applications such as tracking medical devices and objects of daily living. The RF communication link between the reader antenna and tags for indoors exhibits intermittent loss of signal reception due to antenna orientation mismatch and breakpoints within the

antenna coverage area. We propose a design of a sensing platform for tracking objects using a UHF RFID system with passive tags that provides continuous signal reception over the coverage area. We first investigated causes of power loss for passive tags and then designed a sensing platform solution using antenna diversity. The causes of tag's power loss were eliminated with angle and spatial diversity methods that can cover an arbitrary area of interest. We implemented this design in an indoor setting of a trauma resuscitation room and evaluated it by experimental measurement of signal strength at different points and angles in the area of interest. Our sensing platform supported complete coverage and uninterrupted interrogation of tags as they moved in the area of interest. We conclude that this sensing platform will be suitable for uninterrupted object tracking with UHF RFID technology in generic indoor spaces. In addition to the sensing platform, we design an object motion detection system using passive UHF RFID tags attached on medical objects. To use the signal strength for accurate detection of object movement we propose a novel hidden Markov model with continuous observations, RSSI preprocessor, frame-based data segmentation, and motion-transition finder. We use the change in backscattered signal strength caused by tag's relocation to reliably detect movement of tagged objects. To maximize the accuracy of movement detection, an HMM-based classifier is designed and trained with dynamic

settings, and different object types. We deployed an RFID system in a hospital trauma bay and evaluated our approach with data recorded in the trauma room during 28 simulated resuscitations performed by trauma teams. Our motion detection system shows 89.5% accuracy in this domain.

Acknowledgements

I would first like to thank my advisor Prof. Ivan Marsic for this guidance and support. He provided me the opportunity to conduct research that I explored a variety of fields through and truly enjoyed.

I am grateful to Prof. Gajic, Prof. Spasojevic and Dr. Roger for their participation in my thesis committee and valuable comments.

A very special gratitude goes out to Dr. Burd at Children's National Medical center for letting me access the trauma bay.

I am also grateful to my wife and daughter for emotional support in my life. Thanks for all your encouragement.

Dedication

I dedicate this to my mother and father. Thanks for always being there for me.

Table of Contents

List of Figures

1. Introduction

For context-aware systems in indoor work settings, several types of sensors have been applied to capture work activities [1][2][3]. Among the sensors radio-frequency identification (RFID) technology has been used in a variety of areas for its primary function of identifying objects [4][5][6][7]. Additionally, a secondary function of object tracking emerged based on the received signal strength indication (RSSI). A new emerging research area is activity recognition with passive RFID. Our study focuses on motion detection of medical objects as a basis for activity recognition in a trauma bay. The fast-paced, high-risk environment of trauma resuscitation can benefit from a context-aware system, where context refers to the currently performed activity. While most active devices and instruments in a trauma bay such as patient monitoring system, pulse oximeters, and anesthesia machines provide valuable information with physiological data [8], passive devices and tools such as bag-valve mask (BVM), cervical collar, CO_2 detector and etc. need additional sensors to provide information on themselves for the context-aware system [9]. Detecting the motions and identifications of passive objects in the bay can serve as reliable information sources for current tasks and team activities because most medical objects are uniquely associated with

different tasks [10].

The passive RFID tag is one of the sensors that has been used in hospital environments for detecting the status of medical objects due to its more advantageous aspects than other sensors such as active RFID tags and computer vision. Passive RFID technology provides better features for dealing with different shapes and sizes of objects in medical settings. Because a passive tag operates without batteries, it has a very simple structure, requires no maintenance, and is cost-effective and readily applicable to most items including disposable ones. Computer vision has similar characteristics but raises privacy concerns and is less sensitive to small and randomly oriented objects of various shapes than RFID technology whose primary function is identifying objects [11][12]. In the studies [8][13][14][15][16], passive RFID tags are applied to detect the presence of medical objects in the room and not capable of providing information on being used. Moreover these systems are intrusive and require medical staffs to wear RFID readers. In passive RFID systems, continuous reader signal is required because passive RFID tags harvest energy from the interrogation radio signal of a reader to activate. Discontinuities in the reader signal within the working range will cause power loss of the tags. In object tracking applications, it is critical that passive tags receive activation power continuously from the reader signal. If

readers cannot provide passive tags with proper power, the tags will not activate and not respond to reader's interrogation, making the direct tracking difficult. As the working range of UHF RFID is expanded up to 12 meters compared to 1 meter of high frequency (HF) RFID, UHF signals have suffered more for signal discontinuities within the coverage. Several studies have indicated power loss of the passive UHF RFID tags [9][17][18][19].

In this thesis, we present a sensing platform and a motion detection system for passive objects in a trauma bay using passive RFID technology. Our sensing platform design focuses on providing continuous signal reception for tracking objects based on RSSI which is the received signal strength information on backscatter from a passive tag at the reader. The motion detection system uses a hidden Markov model-based classifier and provides information on moving and stationary states of passive medical objects used on a patient bed of a trauma bay. We describe detailed challenges, contributions, designs and performance analysis in separated sections for the sensing platform and the motion detection system.

1.1 Sensing Platform

A UHF RFID reader radio system is a transceiver which transmits and

receive signals simultaneously using the same frequency [20][21]. We investigated the causes of power loss for passive tags and provided a sensing platform solution using angle and spatial diversity of antennas. We applied this platform to a crowded indoor setting of a trauma resuscitation room. The fast-paced, high-risk hospital environments such as trauma resuscitation and surgical operation can benefit from context-aware systems that recognize and analyze currently performed activities. Other studies have used passive RFID tags for tracking medical objects as part of a context-aware system, but provided no specific sensing platforms to deal with power loss of passive tags [13][22][23][24].

In the sensing platform of this thesis, we examine the causes of tag's power loss in indoor environments and present a platform based on a UHF RFID system to provide sensing free of power loss for UHF passive tags. Our key design aim is to provide uninterrupted reader signal over the area of interest with a nonintrusive system. The reader antennas or other related devices of an RFID system should not be in the paths of people's work and equipment movement. The long range of UHF tags allows us to install RFID reader antennas on the room ceiling.

1.1.1 Challenges

To provide uninterrupted reader signal, we investigated the main challenges causing the power loss: human occlusion, indoor multipath fading, and antenna orientation mismatch between the reader antennas and tags. First, because the radio signals of an RFID system cannot penetrate human body, tags occluded by people are rarely activated. To secure different paths of the reader signal, we employed multiple reader antennas located at the room ceiling. The number and exact locations of those antennas are calculated by accounting for the orientation mismatch and the breakpoints. Second, the orientation mismatch causes power loss, leaving passive tags inactivated and unable to provide information to the reader. Because the tag antenna is directional, there is power attenuation due to the orientation mismatch between the reader and the tag. Complete orientation mismatch will result in zero power delivered to the tag. We introduced angle diversity to prevent the power loss from the orientation mismatch. Third, the breakpoints also account for power loss of passive tags. Indoor radio signals undergo scattering, multipath, and delay spread, and the effects of these propagations include constructive and destructive interference [25][26][27]. While the constructive interference strengthens the radio signal, the destructive interference often makes deep fades, called “breakpoints,” in which tags become undetectable

even within the working range [11][25][28]. To cover this effect, we investigated breakpoints and introduced antenna diversity by arranging reader antennas at different angles over the area of interest. To address the above challenges and develop a sensing platform, we first modeled the workspace in our laboratory, because the actual workspace cannot be used for time-consuming system development. We used a commercial off-the-shelf (COTS) system which includes an RFID reader, reader antennas and passive UHF tags.

1.1.2 Contributions

The sensing platform makes three contributions. First, using simulation and experimental measurements we characterized power loss problems and demonstrated that a single antenna cannot continuously track tags within its own range due to breakpoints and orientation-mismatch problems. Second, we presented a sensing platform design of a UHF RFID system with angle and spatial diversity as a solution to the power loss problems and applied it to a crowded indoor space. We then empirically verified the sensing platform by measuring RSSI at different locations and angles within the area of interest. Third, we successfully addressed power loss problems with

continuous RFID data acquisition, eliminating power loss over the area of interest. This sensing platform with small modifications will be suitable for uninterrupted object tracking with UHF RFID technology in generic crowded indoor spaces.

1.2 Object Motion Detection System

Our objection motion detection system provides information on moving and stationary states of passive medical objects attached with RFID tags. Important properties of our system are nonintrusive operation and preserving the privacy of medical teams. For the nonintrusive and privacy-preserving system, we employ the passive UHF RFID tags, whose working range is up to 12 meters. This long range allows RFID reader antennas to be mounted onto the ceiling above the work are. The maximum range of 12 meters is sufficient to interrogate tags from the reader antenna on the ceiling since the height of ceiling is typically no more than 4 meters. To detect movement of medical objects, the received signal strength indication (RSSI) of the tag is used. RSSI is RFID reader measurement of the power in received radio signals from an RFID tag. Since the strength of the received signal varies with the location and orientation of the tag [29][30][31][32], RSSI is a

good indicator for detecting movement of tagged objects. When tag's location or angle are changed relative to the reader antenna, the tag's RSSI at the new location will be different from that at the previous location.

1.2.1 Challenges

When developing a practical system, there are substantial challenges involved: (1) RSSI measurement tends to be significantly affected by the thermal noise at the reader side which results in ambiguous measurement because RSSI directly depends on weak backscattered signal power from the tag. The power of the backscattered signal is typically 10^{-7} to 10^{-5} W at the reader [9]. (2) Although the distribution of RSSI is often assumed as Gaussian [22][33], practically measured RSSI distributions are different from Gaussian due to unpredictable indoor propagations that encumber accurate calculation [34][35][36][37][38]. These varying distributions should be addressed in stochastic processing on RSSI. (3) RSSI measurement from a fast-moving tag over a short interval yields insufficient information on a moving state because the RFID system suffers from severe query-loss [39][40] resulting in lacking of the number of data samples to process noisy RSSI. (4) The device diversity in RSSI measurement causes extra magnitude in RSSI.

Different RFID tags, readers and antennas, even from the same vendor, have different characteristics. Making calibration factors of a number of those devices for each characteristic requires a great deal of handwork. Thus the diversity factors in RSSI measurement should be addressed when using RSSI from multiple devices. (5) Trauma rooms are crowded with people moving around the area of interest, causing interference to radio signals [10] and resulting in noisy RSSI.

We developed a detection system to tackle the above challenges. To tackle Challenge (1) and (2), investigating distributions of RSSI and read rates of multiple tags in the area of interest, the patient bed, we designed RSSI preprocessor to reduce the variance of RSSI distribution introduced by the thermal noise and indoor propagation and make RSSI distribution closely follow Gaussian. Due to Challenge (3) we focus on relative change in RSSI caused by its relocation, rather than absolute values from the moving tag. We introduce frame based segmentation of RSSI data to detect RSSI change and use it for observations of the HMM classifier. Since the HMM classifier makes movement detection on a frame basis, we develop motion-transition finder to determine the exact movement time within a frame based period. To tackle Challenge (4) we create a feature to compensate diversity terms for hidden Markov classifiers. We use difference of RSSI based on a frame basis

rather than using absolute RSSI values. By differentiating RSSI values of two consecutive frames, common extra magnitude of each frame RSSI introduced by diversity factors can be eliminated. To tackle Challenge (5) we develop an HMM classifier based on machine learning. In addition to the interference, each of medical objects has its own usage and frequency of being used, so we create different parameters of the classifier for each object by training in the presence of the interference caused by human moving and environment. Then we develop an augmented HMM classifier from the naive one to increase detection performance further.

1.2.2 Contributions

We make the following contributions: First, we investigate distributions of RSSI in the indoor environment and find out that the distributions randomly vary with locations and have large variances. We propose RSSI preprocessor that process RSSI to be reliable in detecting tag's motion and make accurate approximations to the Gaussian distribution for statistical processing. Second, for the detection system we present a novel method of constructing hidden Markov models with continuous observations, introducing frame based data segmentation and motion-transition finder. The method results in a decrease

in detection error rate by 10.8% compared to naive HMM. Third, we install an RFID system in a hospital trauma bay and evaluate the detection system. This result indicates that the passive UHF RFID tag is a new source of providing not only identification of medical objects but also information on their movement for context-aware systems in hospital settings.

2. Background and Related Work

2.1 Sensing Platform

A study on radio wave propagation and backscatter communication link in an office environment using a network analyzer showed deep fades ("breakpoints") even within a line-of-sight [41]. They demonstrated that a simple statistical channel model in general does not hold for indoor propagation. Another study evaluated the minimum activation power of the tag (–10 dBm) using a anechoic chamber and showed that the signal strength of each UHF RFID channel (50 channels in the range 902.75 – 927.25 MHz) met the –10 dBm turn-on threshold [42]. Based on their results, we localized the breakpoints by measuring the RSSI values in the area of interest and checking if the tag was below the turn-on threshold and did not respond to

interrogation. We used these breakpoint locations as a design parameter of our sensing platform.

Tag's signal power attenuation from orientation mismatch between the tag and reader antenna have been examined [43][44]. These studies, however, provided no design solutions for tag's power loss. Our three-dimensional visualization of their model showed that far-below-the-activation power of the tag at certain angles causes complete power loss, which we also verified experimentally. As a result, in an indoor environment there are breakpoints and orientation mismatches within a line-of-sight that cause tag's power loss in the coverage of a reader antenna.

Previous studies using passive RSSI ranging applied a single reader antenna to cover tags in the antenna range [10][24][26][27]. A single antenna is, however, inadequate to sense tags at all distances from the antenna due to the orientation mismatch and breakpoints, and it is not able to provide continuous tag reading even for tags within its coverage area. On the other hand, studies that used multiple antennas analyzed the dependence of application performance accuracy on different configurations of redundant antennas to determine the proper positions and number of antennas to cover the area of interest [22][39]. However, they did not analyze power loss of a tag nor designed a sensing platform systematically using the antenna

specification. We also used multiple antennas for the area of interest. We, however, investigated radio specification of an RFID antenna and the causes of power loss of passive tags, and provided a sensing platform.

2.2 Object Motion Detection System

In activity and motion recognition several types of sensor such as vision [45][46], accelerometer [47], and RFID tag [8][16] have been used. Although vision-based sensors are not intrusive to medical teams and provides rich contextual information, they raise privacy concerns in the medical domain of our context [22]. Compared to RFID tags whose information is affected by indoor propagation, physical accelerometer data are earned directly though hardwire, so accelerometers are not subject to indoor propagation. They however require batteries and circuitry to work with considerable sizes, resulting in inapplicable to sensitive and small medical objects. Thus the passive RFID tag is decided to use in our system.

In hospital settings for context-aware systems, some of studies used passive RFID tags to detect the presence of medical staff and objects [8], phase of surgical operation [13], nursing activity [14], and clinical intervention [16] but they detect only the presence of tags in their applications without

detecting the movement of objects. When it comes to deciding that objects are used or not, there is no way to detect it with information on the presence. There are some studies on detecting the movement of RFID tagged objects. A study [29] uses sliding windows and sample mean comparison with tag's read rates instead of RSSI. With made-up scenarios they shows, an accuracy of 94% for stationary objects without human presence and moving around the area of interest but the algorithm works poorly for moving objects showing 40 - 65% accuracy. Another study [22] uses a sliding window, multiple RFID antennas and data interpolation and achieves a relatively low accuracy of 80% with people moving around the area of interest.

To increase the accuracy for crowded surroundings, we design and construct a hidden Markov model classifier with continuous observations (RSSI) that can be trained for interference from surroundings. Instead of using sliding window, we develop motion-transition finder for exact detection time and frame based data segmentation to provide uncorrelated observations to the HMM classifier. To statically deal with continuous observations and reduce the variances of noisy RSSI, we investigate distributions, read rates, query missing rates of RSSI and then develop RSSI preprocessor. Our approach achieves an accuracy of 89.5% with four people moving from actual medical activities. Novel designs of HMM classifier and RSSI preprocessor maximizes

the system accuracy in dynamic settings with human moving and improves by about 10.8% in crowded settings compared to naive HMM.

3. RFID Technology for Medical settings

RFID systems consists of tags and readers. RFID tags and readers have to use the same frequency to be able to communicate. Tags are divided into three different types by the frequency band, low frequency, high frequency and ultra high frequency. According to battery use, RFID systems have also two categories, passive and active systems. We examine RFID technology and find applicable RFID systems for medical settings.

3.1 Passive RFID Frequencies

The most common frequencies at which RFID systems operate in the field are low frequency (LF), high frequency (HF), and ultra-high frequency (UHF) bands. Radio waves behave differently at different frequencies so there are advantages and disadvantages in using each band. For example, low-frequency RFID systems which use long wave length have slow data rates and short read ranges but better capabilities of reading on metal or liquid surfaces. High-frequency RFID systems which use short wave length have

fast data rates and long read ranges but are more affected by interference from metal and liquid materials. However with recent RFID technologies, it is possible to use UHF RFID systems on liquids and metals [48].

Low Frequency (LF) RFID System

The LF band frequencies are 120-150 KHz. RFID systems in the band have short read ranges of 10 cm and slower data transfer speeds than higher frequency systems but are less sensitive to radio wave interference.

High Frequency (HF) RFID System

The HF band frequency is 13.56 MHz. HF systems have read ranges between 10 cm and 1 m. Data transfer speed and radio wave interference are moderate.

Ultra High (UHF) Frequency RFID System

The UHF band frequencies are 865-868 MHz in Europe and 902-928 MHz in North America. UHF systems have long read ranges up to 12 m and faster data transfer speeds than LF and HF systems but most sensitive to materials and interference. However there are different UHF tags to work on different materials [49][50][51][52][53][54].

3.2 Passive and Active RFID System

Active RFID System

Typically, active RFID tags have a long life battery that will last a few years to transmit information and run the microchip's circuitry [55] and the range of the active systems is up to 100m. Active RFID systems consist of tags, readers and antennas and typically operate in UHF band. Due to the battery and circuitry the active tags are bigger in size than passive tags and used on large objects such as rail cars and big reusable containers with longer ranges [48].

Passive RFID System

Unlike active RFID systems, in passive RFID systems, the tags have no battery and are powered by a radio signal from readers. With no battery, the passive tags have only a tag chip and antenna and are inexpensive, small in size, and easy to be made in different sizes and shapes depending on applications.

In medical settings, the detecting system should be nonintrusive and RFID

tag's size and shape should be applicable to a variety of medical tools and objects. Thus in this study, a passive UHF RFID system is used due to its long rage and small size.

4. System Model

Our system is designed to detect the motion of medical objects around and on the patient bed in a trauma bay and comprises two parts, a sensing platform that allows continuous data acquisitions from passive UHF tags attached on medical objects, and an HMM-based classifier that provides information on moving and stationary states of passive medical objects under noisy environments. This section describes key design aspects of the system with challenges.

4.1 Sensing Platform Configuration

This section presents a platform based on a UHF RFID system to provide sensing free of power loss for UHF passive tags in indoor spaces. We focus on power loss of tags in indoor environments caused by natural phenomena. We investigated the causes of power loss for passive tags and provided a sensing

platform solution using angle and spatial diversity of antennas. We applied this platform to a crowded indoor setting. Other studies have used passive RFID tags for tracking medical objects as part of a context-aware system, but provided no generic sensing platforms to deal with power loss of passive tags [13][16][22][56]. Our key design aim of sensing platform is to provide uninterrupted reader coverage over the area of interest. For a nonintrusive system, the reader antennas or related devices should not be in the way of people's work and equipment movement. The long range of UHF tags (12 meters) allows installing RFID reader antennas on the room ceiling. To provide uninterrupted reader signal, we investigated the main challenges causing the power loss: human occlusion, indoor multipath fading, and antenna orientation mismatch between the reader antennas and tags. Because the radio signal of an RFID system is absorbed by human body, tags behind people receive insufficient power for activation. To provide alternative paths for the signal power from the reader to the tag, multiple reader antennas are introduced and located at the room ceiling. We found the minimum number and proper locations of those antennas dealing with orientation mismatch and the breakpoints. Another cause of power loss of the tag is orientation mismatch. It makes the tag inactivated and unable to provide information to the reader even though there is no human occlusion.

Because a certain direction of the tag gets close to zero gain, complete orientation mismatch will result in lack of activation power for the tag. We combined angle diversity to the multiple antennas to prevent the power loss from the orientation mismatch. The breakpoints are also another cause of power loss of passive tags. Indoor radio propagation introduces constructive and destructive interference. While the constructive interference enhances reader radio signal power, the destructive interference generates deep fades, called "breakpoints," in which tags become undetectable even within the working range. We investigated breakpoints and introduced antenna diversity by arranging reader antennas at different angles over the area of interest.

In the next sections, we address all the challenges above and design a sensing platform in detail.

4.1.1 Human Occlusion

One of impediments to tracking objects used in work with passive RFID tags is human occlusion. When objects are used during work, it is likely that the direct radio signals of reader antennas will be blocked by people, rendering passive tags unreadable. Because the direct line-of-sight radio signal carries

the most power to activate passive tags but cannot penetrate human body, occluded tags receive insufficient energy to activate. Full occlusion causes loss of signal from tags, while partial occlusion weakens the signal strength and results in flawed information reads. To address these issues, we placed reader antennas where it would most likely have greatest visibility of tags used: on the ceiling above the area of interest. To verify this choice, we observed the work of trauma teams during trauma resuscitation, and found that the ceiling area just above the patient bed best ensured a line-of-sight between reader antennas and tagged medical objects.

4.1.2 Power Loss from Antenna Orientation Mismatch

In typical work scenarios, tagged objects could be oriented in any direction of three-dimensional space. Passive RFID tags harvest energy from radio signals of the RFID reader for their operation. The angle between the tag and reader antenna is at random, and tags could become unreadable at certain angles due to power loss from antenna orientation mismatch. If there is a significant power loss in harvesting energy, tags cannot activate and respond to the reader interrogation. If the tag antenna is directional [57][58][59] and the short side of tag is perpendicular to reader's antenna axis, the power

received by the tag tends to be zero (Figure 1 (a)). The tag parallel to reader's antenna axis receives the maximum power from the reader (Figure 1 (b)).

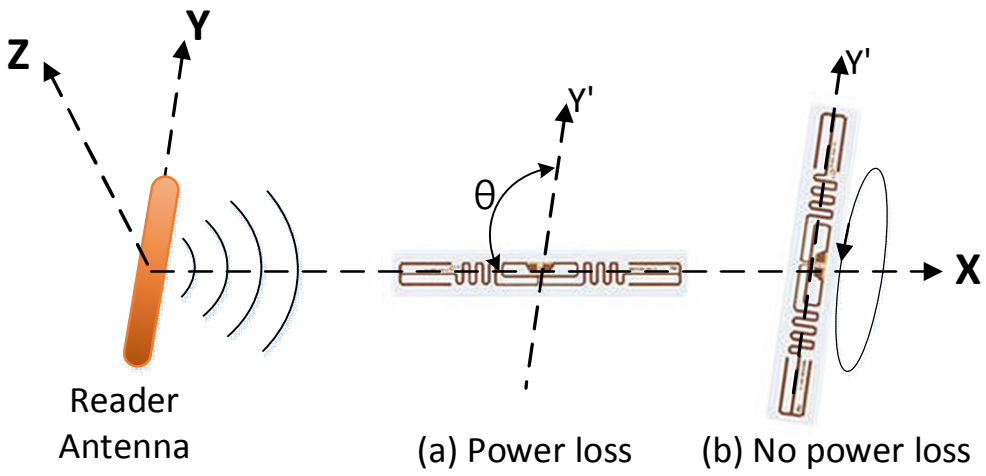

Figure 1. Power loss due to the orientation mismatch between a tag and a reader antenna. (a) The tag perpendicular to the reader antenna receives a minimum power, close-to-zero. (b) The tag parallel to the reader antenna receives the maximum power of reader signal regardless of rotation on the x-axis.

The one-way power loss factor (PLF) [20] and power loss in dB are:

$$\text{Power Loss Factor (PLF)} = cos(\theta) \tag{1}$$

$$\text{Power Loss (PL) in dB} = 20 \cdot \log(\cos(\theta)) \tag{2}$$

where θ is the angle between the reader antenna axis and the direction of tag's long side (Figure 1 (a)).

We modeled the three-dimensional power loss versus orientation using

Equation 2. The color of each patch of the torus in Figure 2 indicates the power attenuation in dB for each direction of RF signal from the reader antenna. In the short-side direction of the tag, the power loss is more than –20 dB while there is no power loss in the long-side direction of the tag.

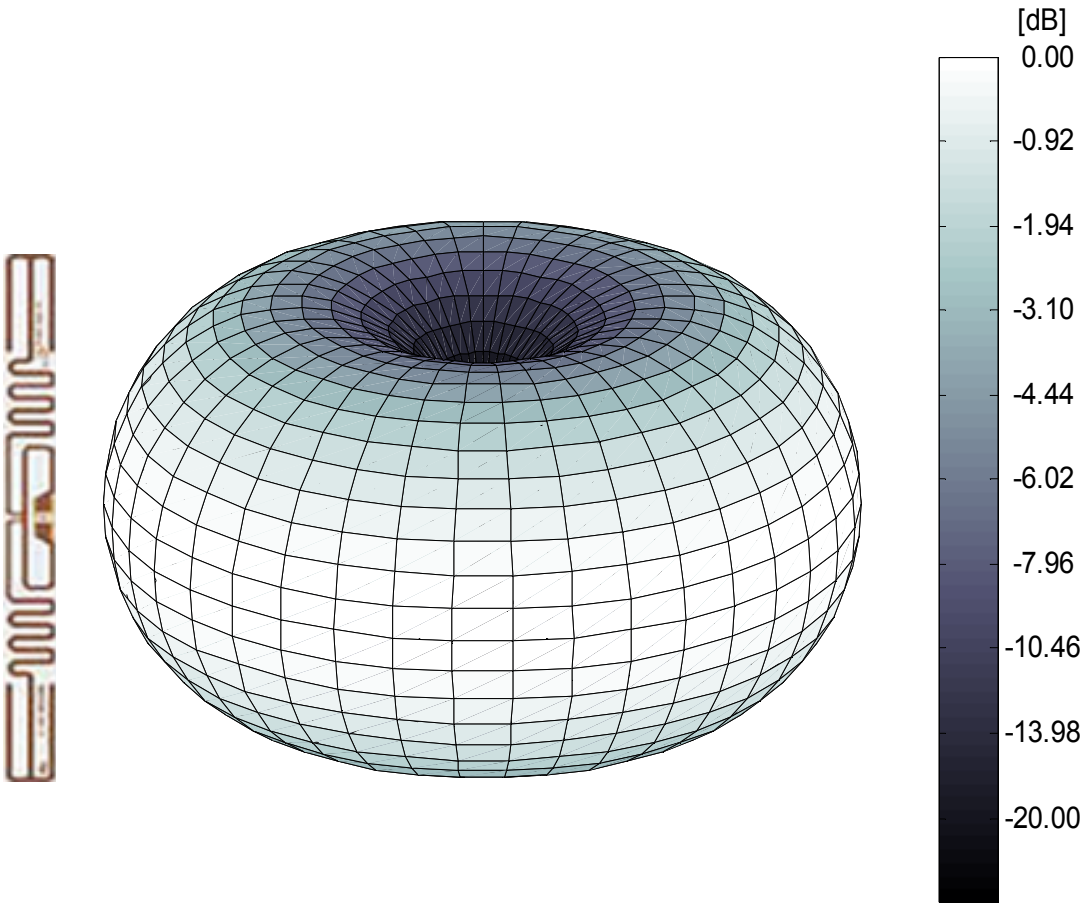

Figure 2. Three-dimensional model of power loss due to antenna orientation mismatch using Eqn.2. The long-side direction of the tag receives the most power and received power in the tag's short-side direction is attenuated by more than –20 dB.

We measured in our laboratory the received signal strength at different tag orientations (Figure 3). All measurements were performed at the same distance of 2 meters from the reader antenna, repeated 150 times for each orientation, and averaged. Zero RSSI is obtained at orientations around 90°, making the tag unreadable due to complete power loss.

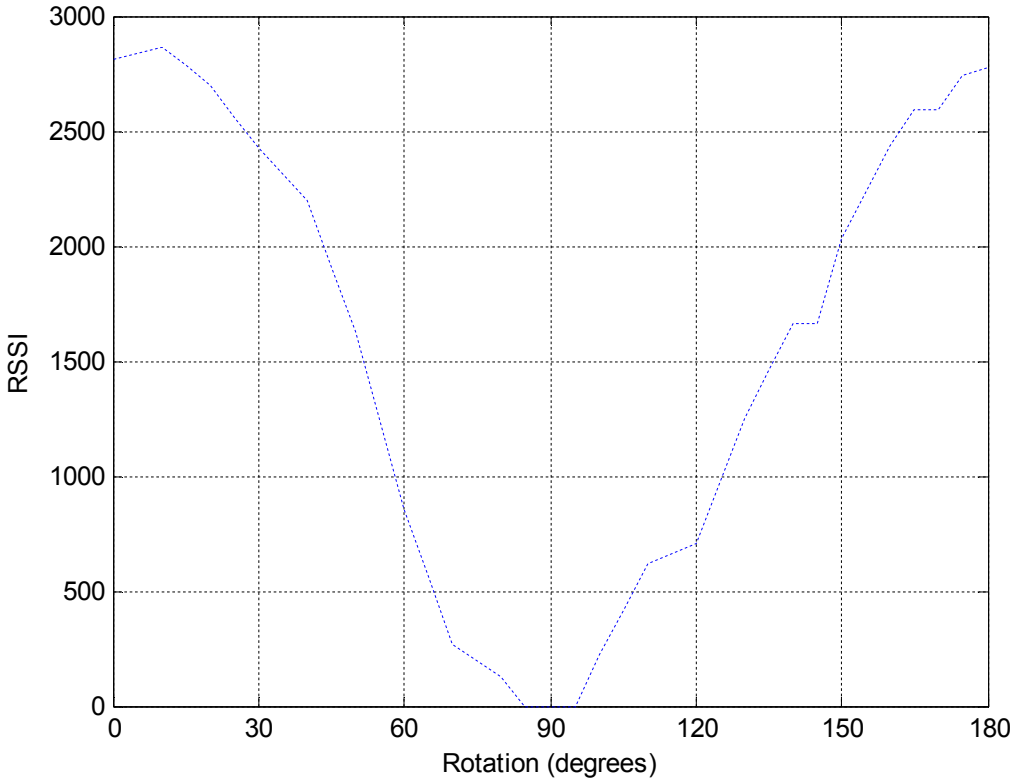

Figure 3. Received signal strength vs. the tag's rotation relative to the reader antenna.

To compensate for zero values of PLF, another reader antenna needs to be placed at an angle different from that between the tag and the first antenna. The antennas should be at different angles to avoid the situation when the tag is perpendicular to both reader antennas simultaneously. There are omnidirectional RFID tags that are insensitive to orientation. They have bigger square antennas compared to slim rectangular antennas of directional RFID tags. However, due to the square shape and larger size, omnidirectional tags may be difficult or impossible to attach to small objects.

4.1.3 Breakpoints

Another source of signal loss for passive tags is due to breakpoints. Breakpoints occur because of multipath fading and cannot be avoided in natural indoor environments [18][25][41]. When a tag is located in a breakpoint, it may be unreadable even within the radio range of the reader antenna. A tag outside of breakpoints usually produces between 90% to 100% query response rate (Figure 4). A tag within a breakpoint receives insufficient signal power to activate and produces low RSSI values and low query response rates, below 50% and down to 0%, depending on how deep the tag is within a breakpoint.

$$\text{Query response rate} = \frac{\text{The number of responses from the tag}}{\text{The number of query attempts by the reader}} \quad (3)$$

To analyze multipath fading [18][19][60][61][62], some studies have used microcell modeling with a ray-based approach [63][64]. A typical ray-based model for the received power is [28]:

$$\frac{P_r}{P_t} = 4 \cdot \left(\frac{\lambda}{4\pi d} \right)^2 \cdot g_r \cdot g_t \cdot \sin^2 \left(\frac{2\pi h_r h_t}{2d} \right) \quad (4)$$

where λ is the wavelength of the RFID frequency, P_r and P_t are respectively the received and transmitted powers, h_r, h_t are the heights of the reader and tag antennas, g_r, g_t are the antenna gains, and d is the distance between the tag and reader antenna.

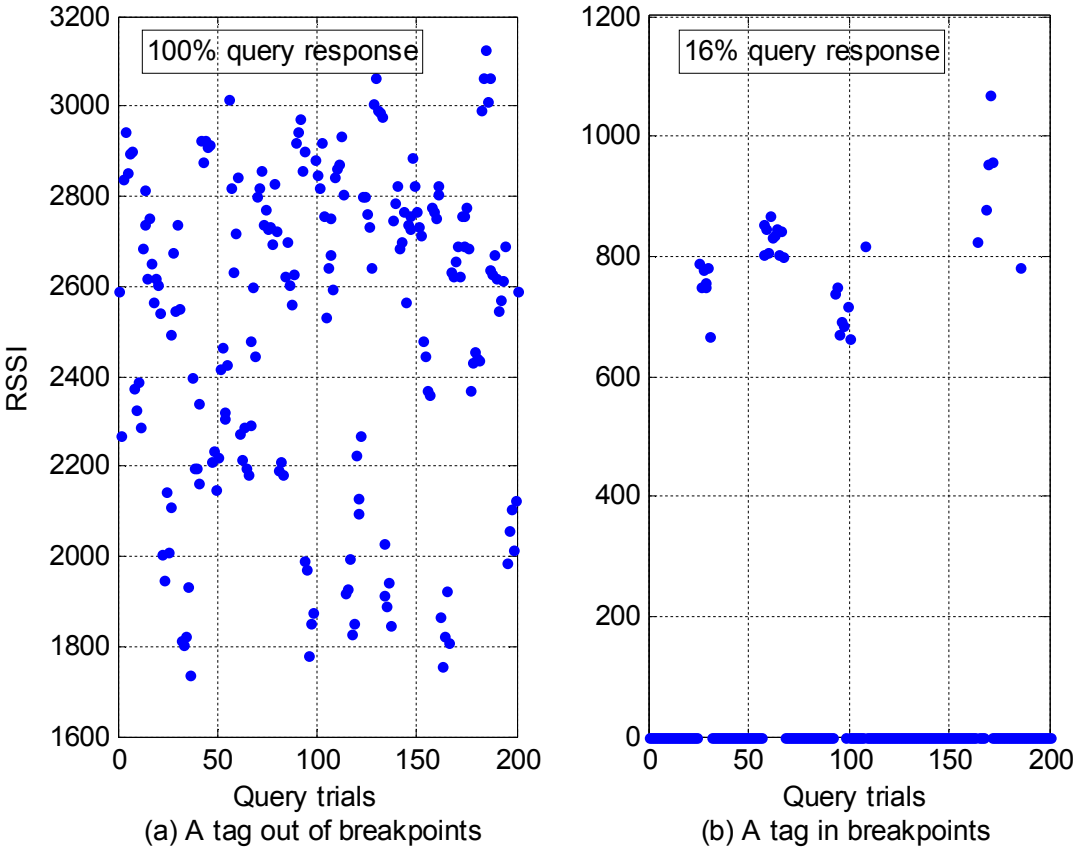

Figure 4. Query response rates for a tag outside of and inside breakpoints (zero values of RSSI indicate no response). (a) Interrogating a tag outside of breakpoints produces all non-zero RSSI values with 100% query response. (b) Interrogating a tag inside a breakpoint produces mostly zero RSSI values with 16% query response.

In our sensing platform scenario, reader antennas are attached to the ceiling and tags are attached to objects used during work, and both antenna types have fixed gains. Thus, h_r, h_t, g_r, and g_t are invariable and Equation 4 can be simplified to Equation 5:

$$\frac{P_r}{P_t} = A \cdot \left(\frac{\lambda}{d}\right)^2 \cdot \sin^2\left(\frac{B}{d}\right) \quad (5)$$

where A and B are constants, λ is the wavelength of the RFID frequency, P_r and P_t are respectively the received and transmitted powers, d is the distance between the tag and reader antenna.

In this model, the parameters that affect the breakpoint locations are the operating frequency and the distance between a tag and a reader antenna. Based on Equation 5, we modeled the breakpoints in Figure 5 according to the distance between the antenna and the tag, with frequencies of 902 and 928 MHz (passive UHF RFID frequency band in the United States is between 902–928 MHz [65]). The UHF RFID band is divided to 50 channels and one of the 50 channels is used randomly for 0.4 seconds. Note that the frequency differences in the UHF RFID band have almost no effect on the location of breakpoints (Figure 5).

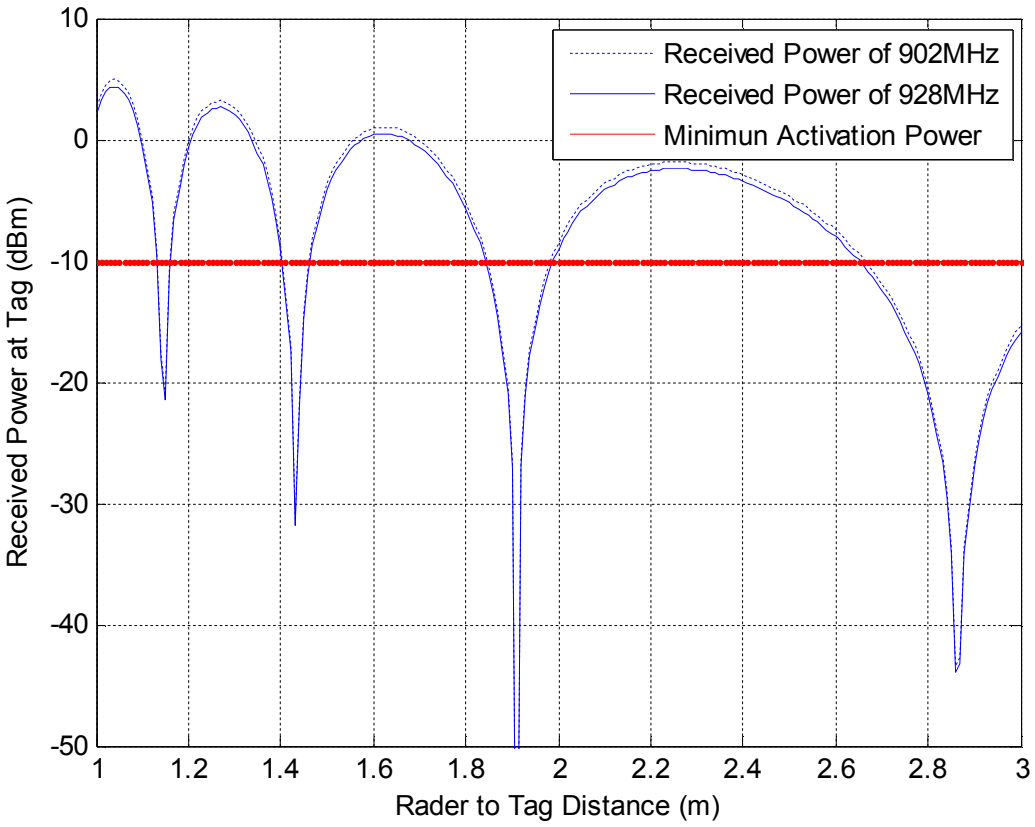

Figure 5. Breakpoints with UHF RFID frequencies of 902 and 928 MHz obtained using the analytical model (Equation 5). The breakpoints are the locations below the minimum activation power indicated by a horizontal line.

This model, however, does not account for reflections and defections by small objects and assumes that scatter is produced by large flat surfaces such as walls [9] and the breakpoints could be inconsistent from the actual breakpoints for indoors environment with furniture and other objects. Therefore, we estimate breakpoints by measuring RSSI values in the area of

interest. From the examination of the human occlusion the reader antenna is supposed to be located on the ceiling area right above the working area, a patient bed, for the setting. We measured RSSI values with the reader antenna at four different locations that make angle diversity for tackling the antenna orientation mismatch problem. The four locations are right above one third and two third of two long sides of the working area rectangle. The measurement of the signal strength is taken within the area of interest to track tagged objects with uninterrupted reading of passive RFID tags. Figure 6 shows RSSI versus distance from the four observed locations; zero RSSI values indicate breakpoints. Figure 7 indicates how a reader antenna and tag are located in this measurement. Because antenna heights and gains are fixed and only the antenna location of the working area is changed within the area of interest, the varying of the breakpoints from the four observed locations remains within 8 cm. Experimentally measured breakpoints from the four locations appear at 0.28 and 1.08 meters with a tolerance of ± 4 cm. From this measurement we then define the locations of breakpoints and the reader antenna coverage on the patient bed height level to design the sensing platform. The location of breakpoints is 0.28 m from the reader antenna and the antenna coverage is considered to be 1.01 m (Figure 9 (b)). We include a margin for stability because the distance between the end of the second

breakpoint (110 cm) and the actual coverage boundary (130 cm) is quite short with close-to-zero-power areas. Due to breakpoints one antenna for one zone does not fully cover its reading range and another antennas are need to compensate each other's breakpoints. Breakpoints can be avoided by spatial diversity that employs multiple antennas at different positions. The next section describes our sensing platform design that tackles the above impediments for using passive UHF RFID.

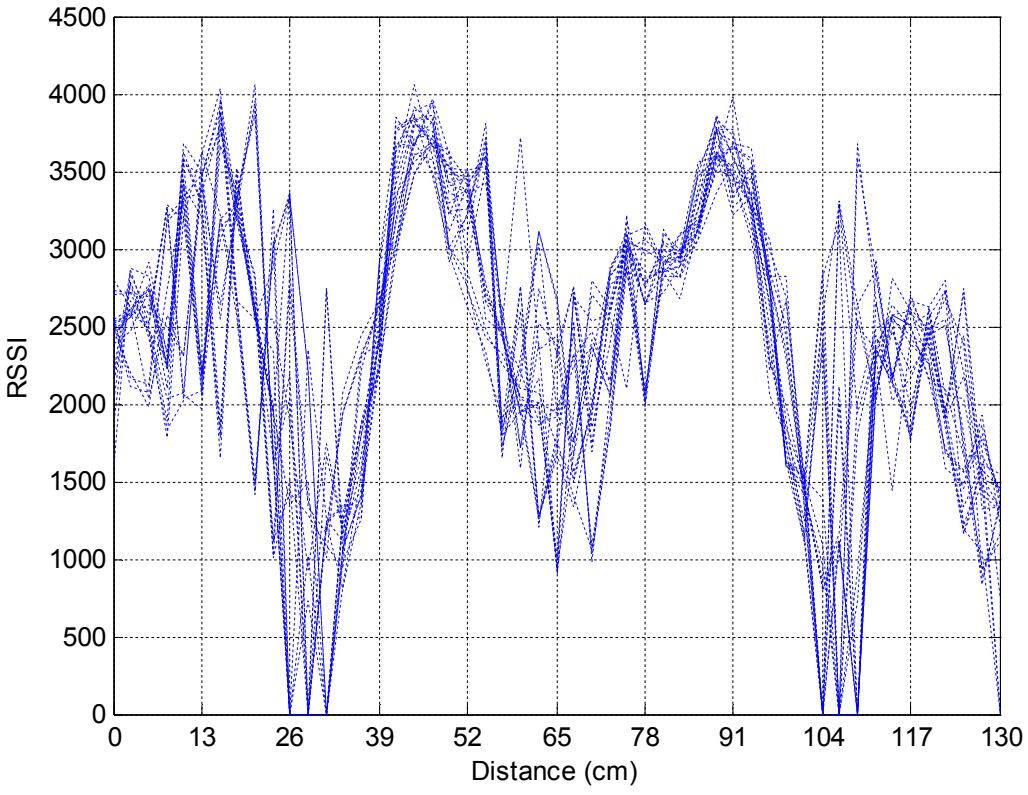

Figure 6. Measured RSSI versus the tag distance from the origin right under the reader antenna from the setup (Figure 7).

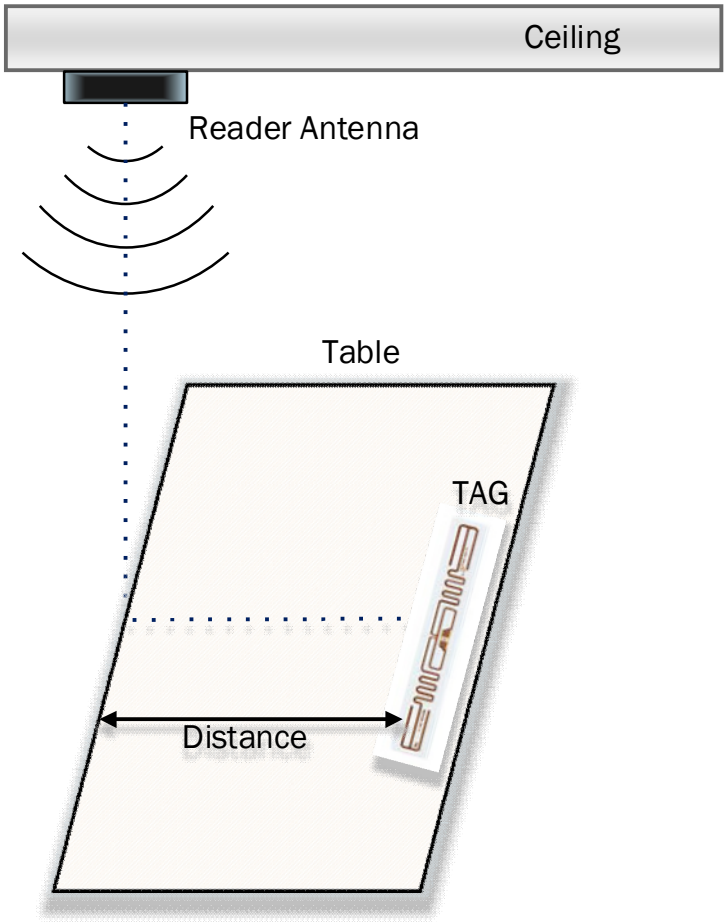

Figure 7. The setup for measuring RISS is molded as a trauma bay. The reader antenna is on the ceiling at 2.65 m high, facing down to the floor. The tag is at 0.76 m above the ground and moved horizontally over the distance of up to 1.3 m away from the origin.

4.2 Sensing Platform Design

As mentioned, physical phenomena and human occlusion during the handling of tagged objects hinder continuous reading of passive RFID tags. These impediments constrain the location of reader antennas to the ceiling area and require antenna diversity to mitigate the power loss from orientation mismatch and breakpoints. Another constraint is the distance between the reader antenna and the area of interest because the coverage area of interrogation signal is proportional to the distance to the tag (Figure 8). Single-room indoor environments usually restrict the coverage area. For example, at 1.9 m distance between the reader antenna on the ceiling and RFID tags on a desk, the coverage area is a circle of radius 1 m. Our theoretical solution for antenna configuration is derived to meet the following requirements:

R1: The area of interest should be completely covered by at least two antennas to achieve (i) angle diversity and eliminate orientation mismatch of the reader and tag antennas, and (ii) spatial diversity to eliminate breakpoints.

R2: Breakpoint regions of different antennas must not overlap to avoid

any remaining breakpoints.

R3: The number of antennas should be minimized because of cost and esthetic reasons.

Although our method works for any shape of the area of interest, for simplicity we assume a rectangular area of length ℓ and width w (Figure 9 (a)); in our target domain of trauma resuscitation ℓ is 2 m and w is 0.75 m. The beam pattern of a reader antenna is cone-shaped (Figure 8) [66], and that all reader antennas have identical coverage (1.01 m radius) and breakpoints (single circle of 0.28 m radius), as shown in Figure 9 (b). To meet Requirements R1–R3 under the given assumptions and parameters, we use a geometric approach in determining the adequate number and positions of the reader antennas. Given the identical characteristics of reader antennas, any irregular positioning of antennas would require more than necessary antennas (violating Requirement R3) or would have gaps in coverage (violating Requirement R1). It follows that only a regular positioning of antennas would meet all the requirements (Figure 10 (a)). There are three regular tilings of the plane [67]: the triangular tiling, the square tiling, and the hexagonal tiling, which can be obtained by composition of triangular tiles

(Figure 10 (c)). It is known that the hexagonal tiling (and, by extension, the triangular tiling) produces the densest circle packing in the plane [67], which means that it packs the greatest number of antennas of all regular tilings. To meet Requirement R3, we chose the square tiling to cover the area of interest which produces the least dense circle packing. Therefore, we met Requirements R1–R3, addressing the problems of breakpoints and orientation mismatch (Figure 10 (d)).

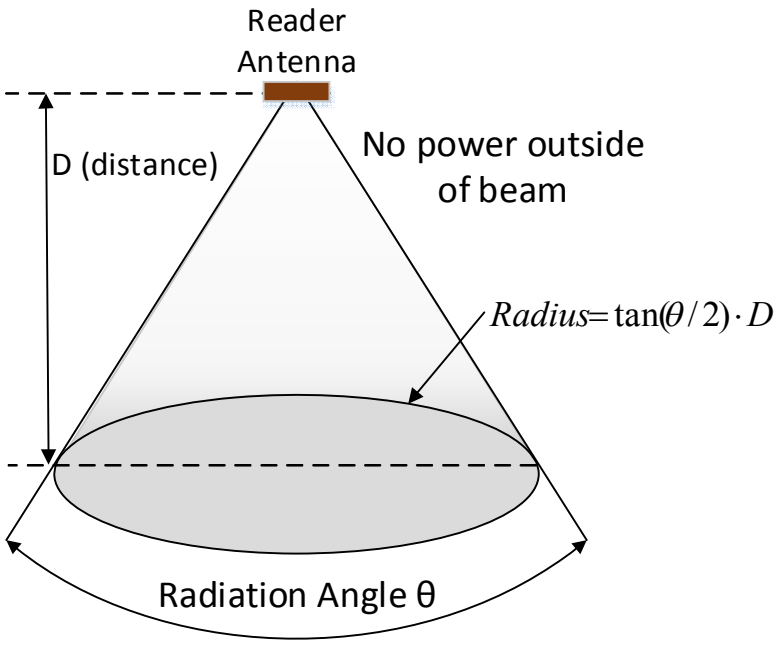

Figure 8. Radio signal Radiation approximation for a directional reader antenna.

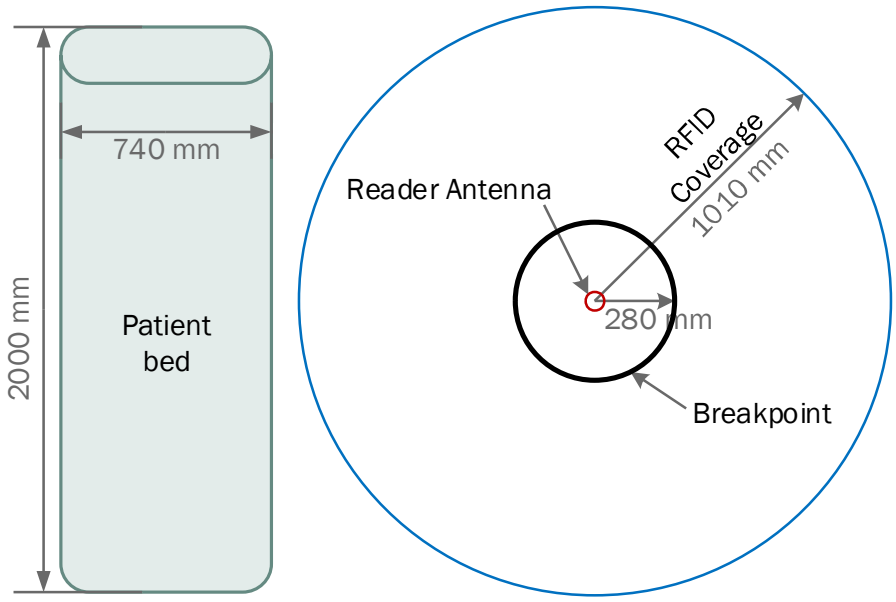

Figure 9. (a) The size of the patient bed. (b) Top view of reader's antenna coverage with one breakpoint.

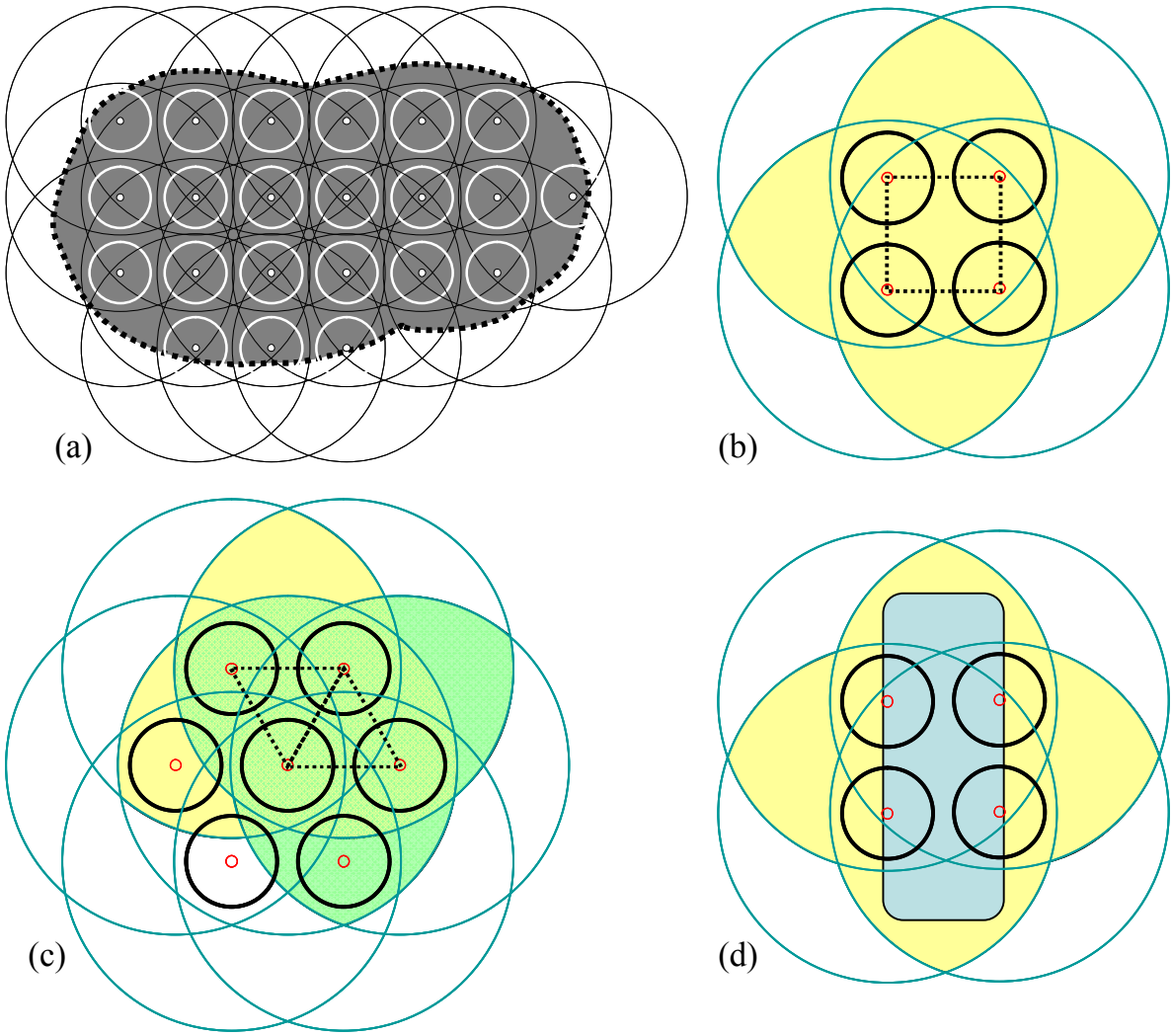

Figure 10. (a) Regular tiling of an area of interest to eliminate breakpoints by covering with at least two antennas for spatial diversity. (b) Shaded coverage area achieved using four antennas in a rectangular tiling. (c) Shaded coverage area achieved using four antennas in a triangular tiling, which combined makes hexagonal tiling. (d) Four antennas arranged in rectangular tiling cover the whole working area with at least two antennas, achieving antenna diversity with a sufficient margin.

4.3 Experimental Results

4.3.1 Hardware Setup for the Sensing Platform

We built the sensing platform using commercial off-the-shelf (COTS) equipment from Alien Technology which include an RFID reader ALR-9900, four circularly polarized antenna ALR-9611-CRs and passive UHF tag ALN-9740. The operating frequency range of the system is 902.75 – 927.25 MHz with frequency hopping. The number, spacing and dwell time of hopping channels are 50, 500 KHz, and <0.4 seconds, respectively. The power of RF transmitter is ≤30 dBm. The reader antenna dimensions, gain and beam width are 28.4×19.5×4.3 cm, 6 dBi max, and 40°. The dimensions and read range of the tag are 98.2×12.3×0.08 mm and up to 12 m [43]. The RFID reader and a desktop computer were connected with network cables to a router for TCP/IP communication. The reader provided RSSI and ID of passive tags and was not capable of detecting phase of tag's signal. The communication protocol between the reader and the passive tags is the EPC Class-1 Generation-2 standard [68]. The sensing platform developed in our lab (Figure 10 (d)) was deployed in trauma bay of a Level 1 trauma center (Figure 11). The four antennas were attached on the ceiling at 2.65 m height, facing down to the floor, 75 cm apart from each other along each horizontal

axis.

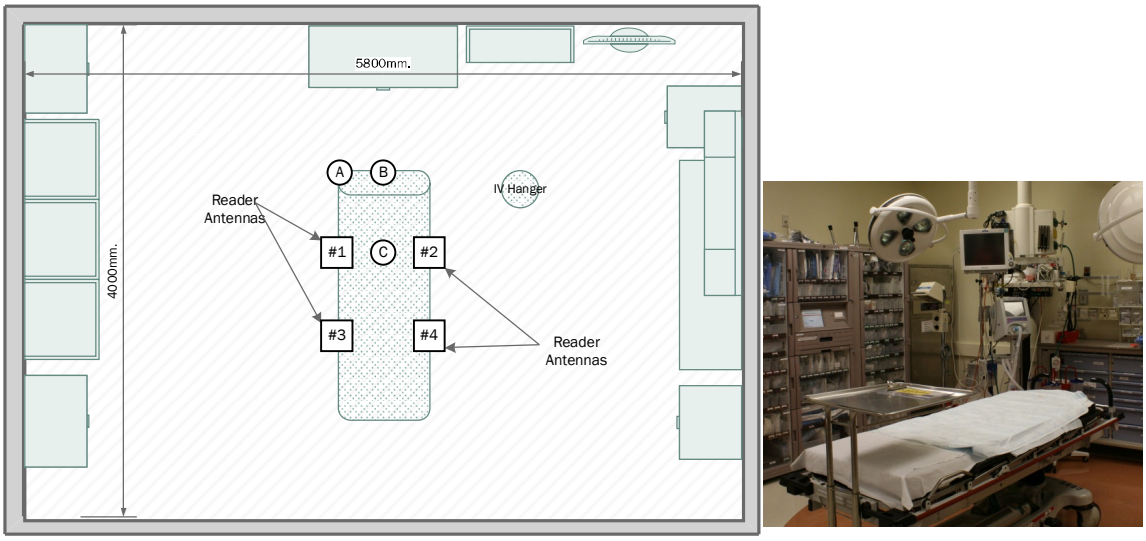

Figure 11. Trauma bay floor plan with four antennas on the ceiling. RSSI was measured at Points A, B and C to verify our design for angle diversity.

4.3.2 Experimental Results of Angle Diversity

To verify the antenna angle diversity for the area of interest around the patient bed, we measured how RSSI's depends on tag's orientation at points A, B and C (Figure 11). Points A and B were chosen within the area of interest at the greatest distance from the diversity antennas. Angle differences at larger distances are smaller, which means that points A and B

were the worst-case points for angle diversity. Point C was chosen so that two antennas (#1 and #2) and the tag were lying on a line, although the tag was at a lower height. Point C was also in the range of antennas #3 and #4 (Figure 11), which were other diversity antennas for this point. Since other points in the area of interest were relatively symmetrical to the reader antennas (Figure 11), Points A, B and C represented all the worst-case points for angle diversity. Figure 12 shows how RSSI depends on tag orientation at these three points. The RSSI was measured 150 times at orientation increments of five degrees and then averaged. Zero RSSI indicated zero power due to complete power loss from antenna orientation mismatch. None of zero RSSI angles at Points A, B and C overlapped. Therefore, our sensing platform eliminated zero-power points for all orientations of the tag in the area of interest.

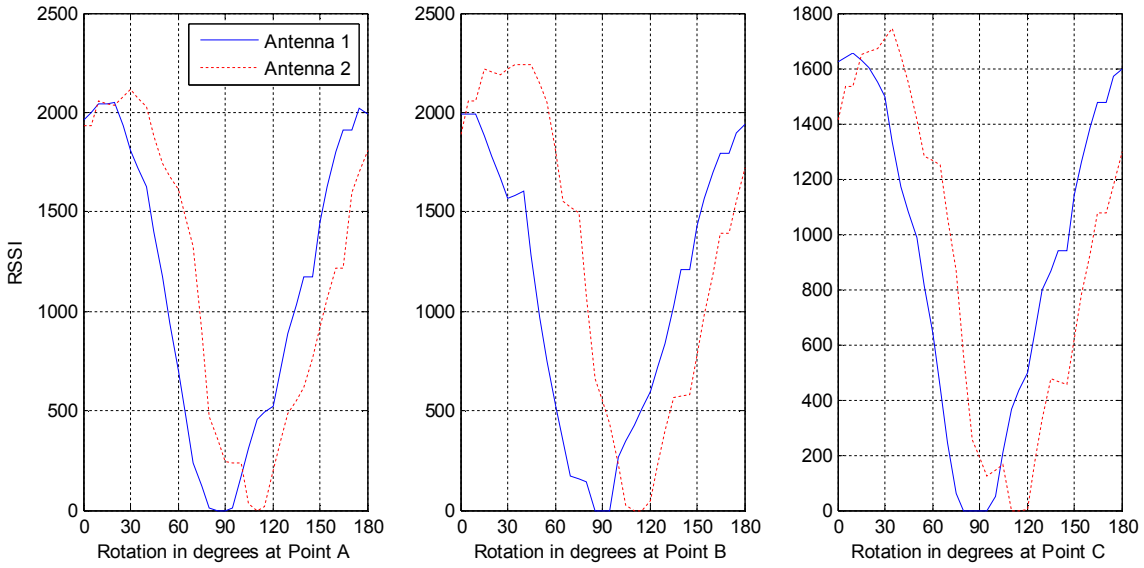

Figure 12. RSSI as function of tag rotation at Points A, B and C from reader antennas #1 and #2 (Figure 11). Zero degrees indicates that the tag's long side pointed to the reader antenna #1, as in Figure 1(b).

4.3.3 Experimental Results of Covering Breakpoints

We measured the four circular breakpoints in the area of interest (the patient bed) covered by the four antennas (Figure 10 (d)). The measurements were obtained so that one antenna at a time was activated and a tag was moved along the y-axis on a grid (Figure 13) over the patient bed, with tag's long side facing the active antenna. For each location, query response rate was acquired with 500 trials. Breakpoints were identified as the points where the

measured query response rate (Equation 3) was below 25%. Finally, all four antenna centers were aligned, and their breakpoints superimposed to specify the maximum areas of breakpoints. The furthest breakpoints occurred at about 36 cm from an antenna (Figure 13). Therefore, if the distance between antennas is greater than 72 cm, there will be no overlaps of breakpoints. Because in our sensing platform (Figure 10 (d)) the antennas are at 75 cm apart from each other, their breakpoints did not overlap and Requirement R2 was fully met.

Note that the widest breakpoints appeared about 8 cm wide along the central direction of each antenna beam (Figure 13), facing the center of the patient bed (Figure 10 (d)). The breakpoints on edge directions of the bed were sparse and narrow. The bed edges were less affected with breakpoints, because they experienced fewer reflected radio signals than the central area of the bed.

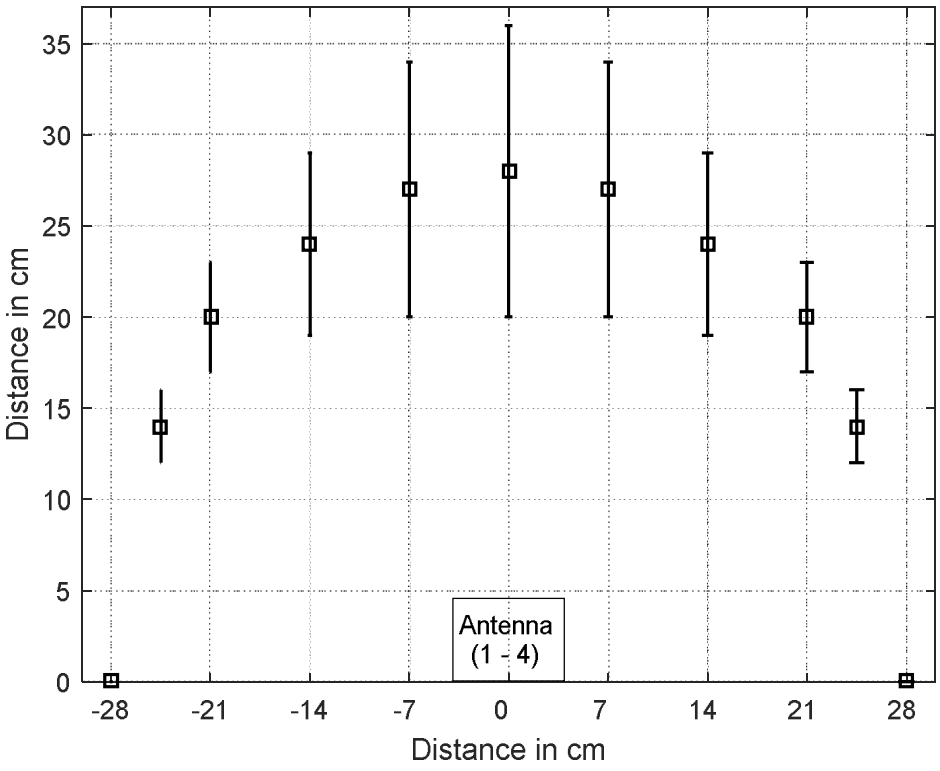

Figure 13. The breakpoints measured from the four antennas on the patient bed (Figure 10 (d)) are overlapped. Each antenna is located in the origin labeled with a box "Antenna". Each error bar indicates the width of a breakpoint.

4.4 Discussion

The experimental results at different locations and angles in the area of interest show that power interruption of the tag is covered by angle and spatial diversity methods. We conclude that this design of the sensing platform will provide continues object tracking without losing power of the

tags in indoor environments.

4.5 Analysis and Processing of RSSI

We use received signal strength indication (RSSI) of passive UHF tags for detecting the motion of medical objects. RSSI is a power measurement at the reader device of a received radio signal from a tag. Because the strength of the received power depends on the distance between a reader antenna and a tag, RSSI is a good indicator of moving objects. However, in a system based on passive RFID tags, estimation of RSSI for mapping the power strength to distance is inherently low accuracy [11][12][69] because RSSI relies on the weak backscattered signal power that is easily affected by the thermal noise on the receiver side. As a result, the practically measured RSSI has considerable large variances [33][63]. In this section RSSI is analyzed and processed to use in an HMM classifier.

4.5.1 RSSI Read Rate with Varying Tag-set Size

We studied the effects of different tag-set sizes on read rates and query-missing rates (Equation 6) because we are tracking multiple objects in the area of interest simultaneously.

$$\text{Query-missing rate} = \frac{\text{The number of missing responses from the tag}}{\text{The number of query attempts by the reader}} \quad (6)$$

We used an Alien Technology reader that provides RSSI in a 16-bit resolution, covering a maximum read range of 12 meters. Based on observations of our target domain (trauma resuscitation), we found that up to ten tagged objects can be used simultaneously in the work area (patient bed). Many more tagged objects may be present in the room, but are normally kept outside of the work area to avoid clutter. Therefore, relatively a small number of objects are within the coverage of antennas focused on the work area. EPC Class-1 Generation-2 standard [70] supports a multi-access method for multiple-tags interrogation using a variation of slotted Aloha protocol [71]. The read rate is the number of tag interrogations per second. Queries might be missed because of collisions when multiple tags respond simultaneously and errors in wireless backscatter communication.

We dispersed a set of tags randomly in the area of interest (around 2 meters from the reader antenna), aligned tag antennas parallel to the reader antenna to maximize the read rate, and left the tags stationary. The reader was commanded 1,000 times to interrogate all tags within the range. As the

tag-set size increased, the total number of reads per second initially increased, but then decreased around the tag-set size of 30, while the read rate per single tag monotonously decreased (Figure 14). We observed a decrease from 30.8 interrogations per second with a single tag to 14.2 per second with 10 tags. Query-missing rates for tag-set sizes up to 10 tags appeared not to depend on the tag-set size and remained below 3% (see Figure 14, units on the right side of the chart). Reading rates for larger tag-set sizes, with 50, 100 or more tags, are very low, but as noted earlier, such large tag-sets usually do not appear within the work area. This results show that how many RSSI data can be obtained with varying tag-set size in a fixed time period.

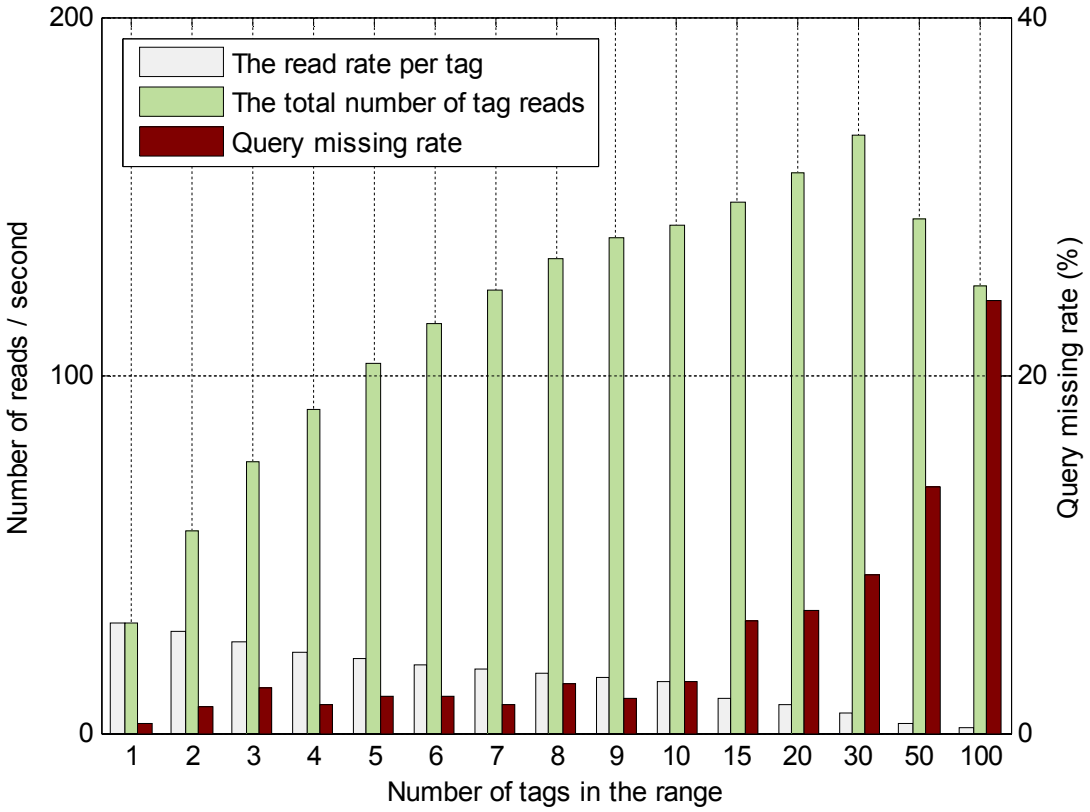

Figure 14. Read rates and query-missing rates according to the number of tags at around 2 meters from the reader antenna. Note the read-rate units on the left side and query-missing-rate units on the right side of the chart.

4.5.2 RSSI Distribution

We investigated the distributions of measured RSSI data and then process RSSI to use in our classifier. Figure 15 shows the noise level of the RSSI values. The RSSI samples were captured from a tag at a single distance in a real trauma bay. The maximum fluctuation is about 60% of its mean. Figure

16 is the power spectrum of raw RSSI values acquired from a stationary tag and shows the noise of the RSSI is crowded mostly around the DC level. The tag read rate is 30 / second. In practice, two sets of RSSI data taken at two adjacent locations largely overlap because of noisy RSSI characteristics. When mapping RSSI values with respect to tag's location, such overlap results in detection errors and inability to differentiate a location form another location. Figure 18 (a) shows two measured RSSI data distributions, each averaged over 18 locations. For example, using raw RSSI data the error probability for the detection of a 5 cm movement is 0.38, which is close to the maximum error probability of 0.5. This big error rate due to the large distribution of RSSI is one of challenges to use noisy RSSI in location mapping. We tackle the challenge in the section after Probability Distribution of RSSI.

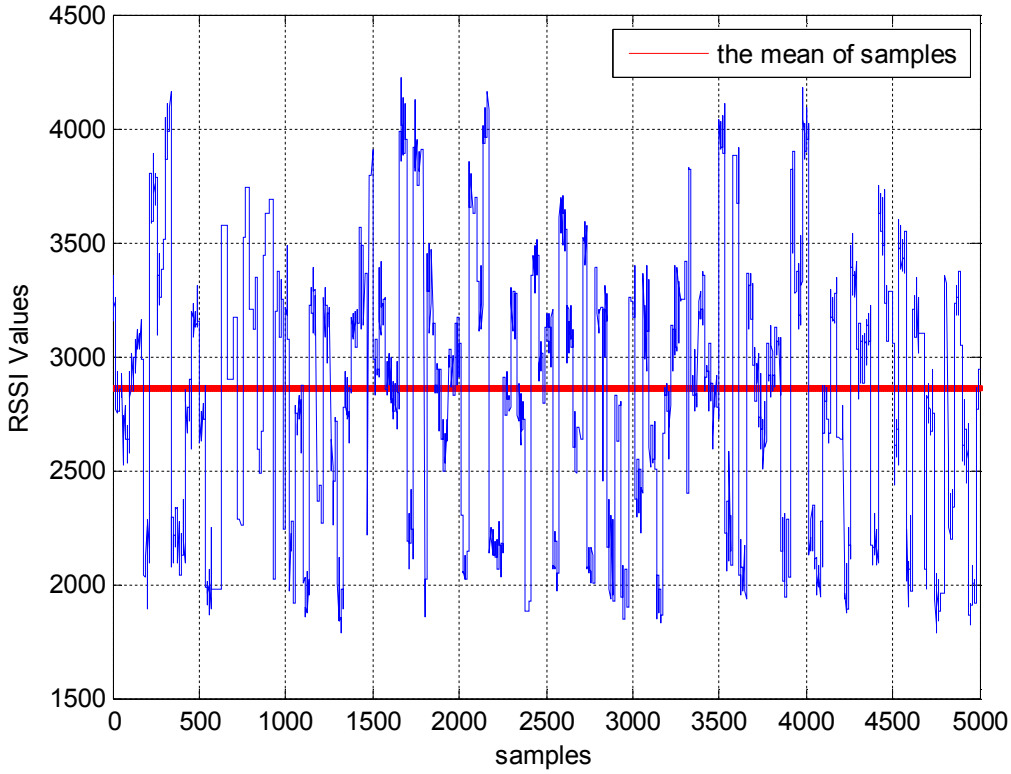

Figure 15. RSSI values from a stationary tag captured in a real trauma bay.

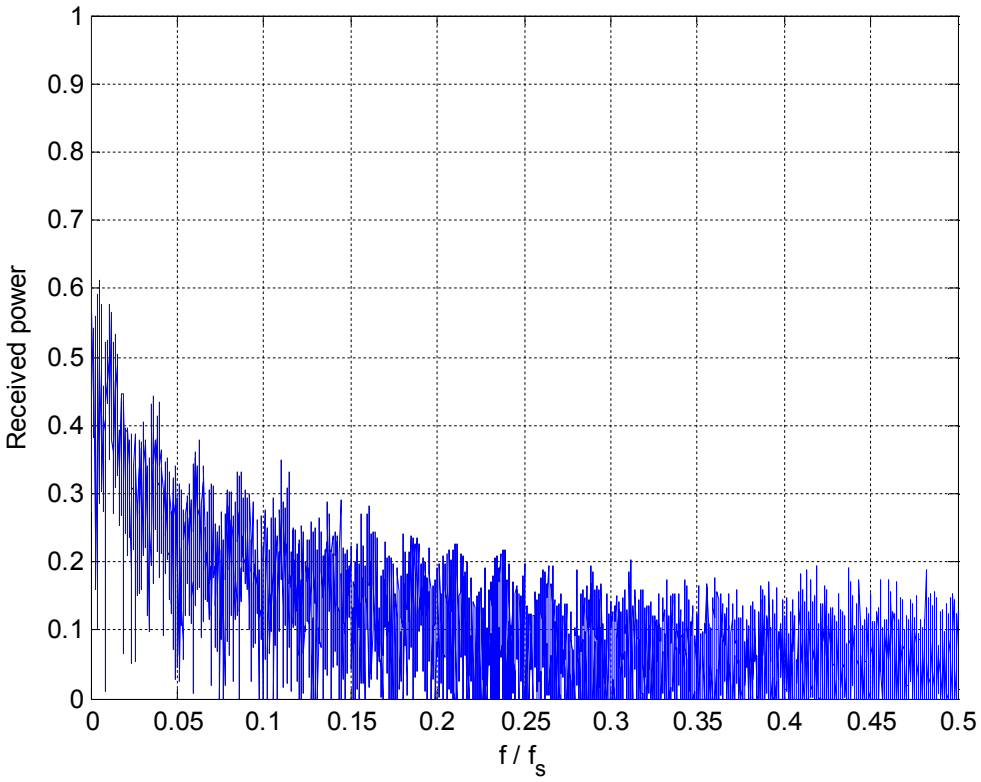

Figure 16. The power spectrum of RSSI values from a stationary tag

4.5.3 Probability Distribution of RSSI

In order to use RSSI in a classifier system, a predictable probability distribution of RSSI is required. Probability distributions play a great role in classification. We gathered RSSI reads from 18 different locations on the area of interest which is a patient bed and drew their frequency distributions in Figure 17. While a few of the distributions look like Gaussian, the others are unpredictable and widely different to each other. Thus we build a predictable

probability distributions of RSSI regardless of locations and take care of the large distributions of RSSI by processing RSSI in the next section.

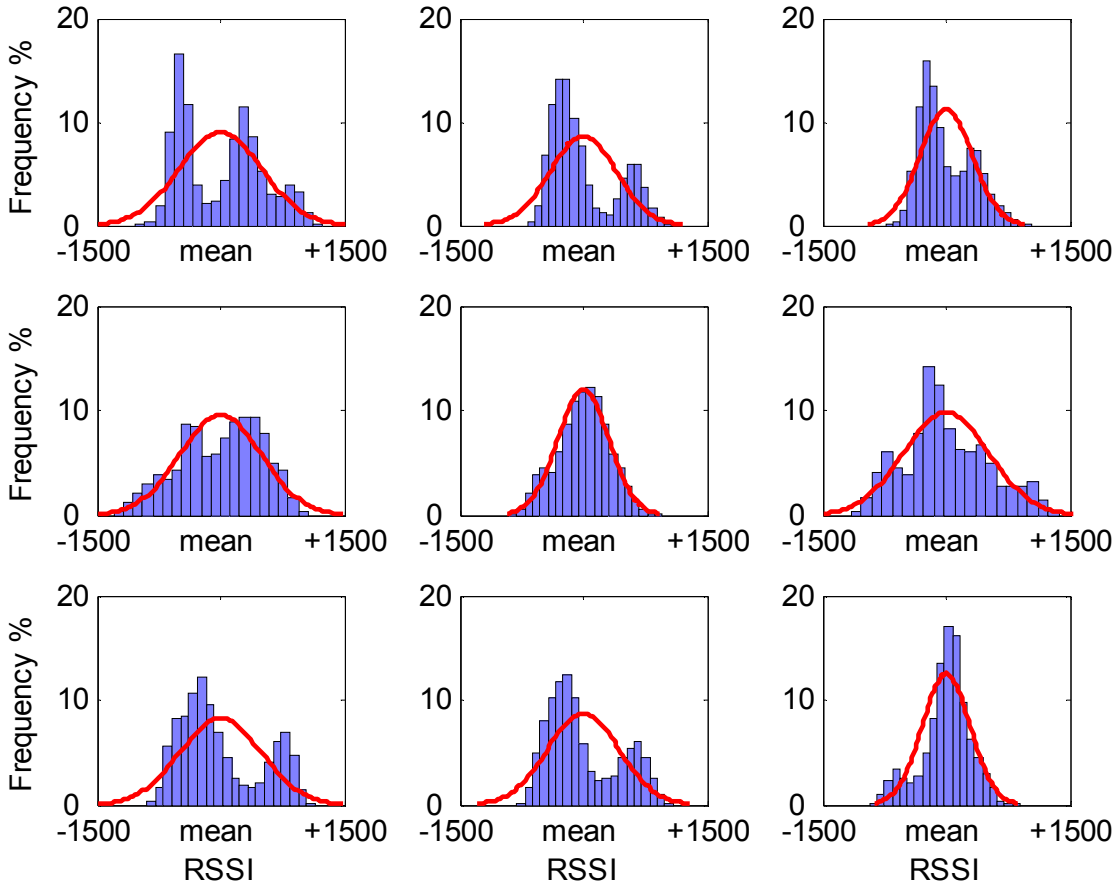

Figure 17. Distributions of measured RSSI at different locations in the area of interest (9 locations out of 18 are shown), where each set contains 10,000 samples. The bell curves are fitted Gaussian distributions.

4.5.4 RSSI Processing

We observed that RSSI distributions in the area of interest are very large for cm-location mapping and the probability distributions are not unique and unpredictable due to varying from one location to another location. Because a hidden Markov model classifier requires probability distributions of observations (RSSI) to compute the most-likely corresponding sequence of state, the probability distributions of RSSI in any location of the area of interest should be known.

The desired properties for the RSSI after processed in our context are: (a) The lag of the processing is predicable; (b) The processing should not smear out sharp transitions in the data; (c) The processing must work for nonlinearly moving objects in crowded rooms; (d) the processing should reduce the RSSI distributions; and (e) the processing should provide predictable probability distributions.

To meet the properties, we applied the Central Limit Theorem (CLT) as a RSSI preprocessor. The CLT allows obtaining accurate approximations to the Gaussian distribution associated with sums of random variables [72]. As the sample size N increases (typically $N \geq 30$), the distribution of the sample

averages, $\bar{x}$, converges to the normal distribution [73] (Equation 7 - 9).

$$\mu_{\bar{x}} = \mu_x \tag{7}$$

$$\sigma_{\bar{x}}^2 = \frac{1}{N}\sigma_x^2 \tag{8}$$

$$\bar{x} = \frac{1}{N}\sum_{i=1}^{N} x_i \tag{9}$$

where $x_1, \ldots, x_N$ are random variable samples with mean μ_x and variance σ^2_x.

Another advantageous property of the sample average $\bar{x}$ is to reduce the variance by a factor of *N*. Each RSSI read is a random variable with a mean that represents the received power strength. Equations 10 and 11 show that the variance of the sample average of noisy RSSI is proportional to one over the number of subset samples:

$$\frac{1}{n}\sum_{i=1}^{n} S(i) + V_i(i) = S_{mean} + \frac{1}{n}\sum_{i=1}^{n} V_i(i) \tag{10}$$

$$\hat{\sigma}_v^2 = \frac{1}{n^2}\left(\sigma_{v_1}^2 + \sigma_{v_2}^2 + \ldots + \sigma_{v_n}^2\right) = \frac{1}{n^2}\left(n\sigma_v^2\right) = \frac{1}{n}\sigma_v^2 \qquad (11)$$

where n is the number of inputs, $S(i)$ is a RSSI value without noise, $V(i)$ is a uncorrelated Gaussian random noise with zero mean and variance σ_v^2 in raw RSSI, and $S(i) + V(i)$ represents noisy raw RSSI.

With increasing sample size N the RSSI variance decreases at a rate of $1/N$. However the sample size N needs to be balanced because short RSSI transitions from fast movements might be averaged out. We found that the minimum required distance for detecting object's motion is 5 cm by observing trauma resuscitations which is our application domain. With setting a condition that the overlap of processed RSSI distributions at two 5-cm-apart locations is close to zero (less than 1%) we determined that the minimum sample size ($=N$) equals 110 by calculating the overlap with processed RSSI. Figure 18 (b) shows that the overlapped processed RSSI values are 0.88% with the sample size 110. The smallest read rate for the tag-set size up to 10 is 14 reads/sec (Figure 14), so approximately 8 seconds are needed to read at least 110 samples. Therefore, we used an 8-second window for RSSI preprocessor. In the cases of fewer than 10 tags in the range there should be more than 110 samples in an 8-second window and this will results in smaller overlap areas than that from 110 samples. Figure 19 shows the

processed RSSI distributions with the sample size of 110. Unlike the measured RSSI distributions (Figure 17), the processed RSSI distributions at all locations make very close approximations to the Gaussian distribution, because of the CLT. The standard deviations of the estimated RSSI data are between 0.8% and 5.8% of the mean, an average of 2.3%. The estimator reduces the standard deviation of measured RSSI to 14.6%. The variance of processed RSSI is reduced to 14.6% of the variance of measured RSSI and the distribution of processed RSSI is Gaussian. We used processed RSSI for our detection system as an input.

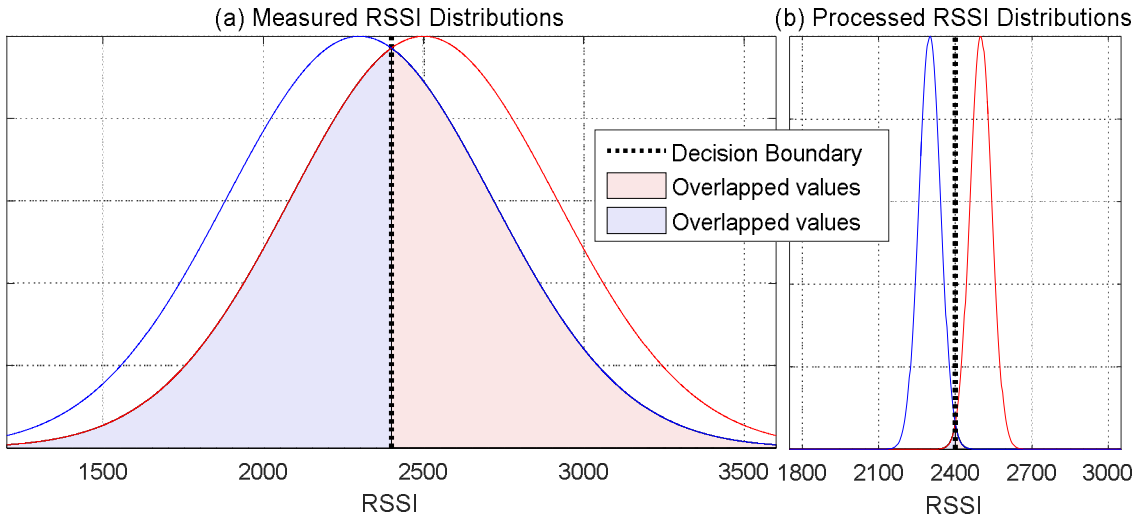

Figure 18. Distributions of measured RSSI and processed RSSI from 18 pairs of different locations, shown as bell curves. In both charts, the left bell curve shows distribution averaged from 18 locations used in Figure 17 and the right curve shows distribution from 18 tandem locations, each 5 cm apart from the original. The decision boundary (thick dotted line) is set to be the

midpoint of the means of two distributions. (a) The measured RSSI data distributions overlap by 38%. (b) The distributions of processed RSSI values overlap only by 0.88%.

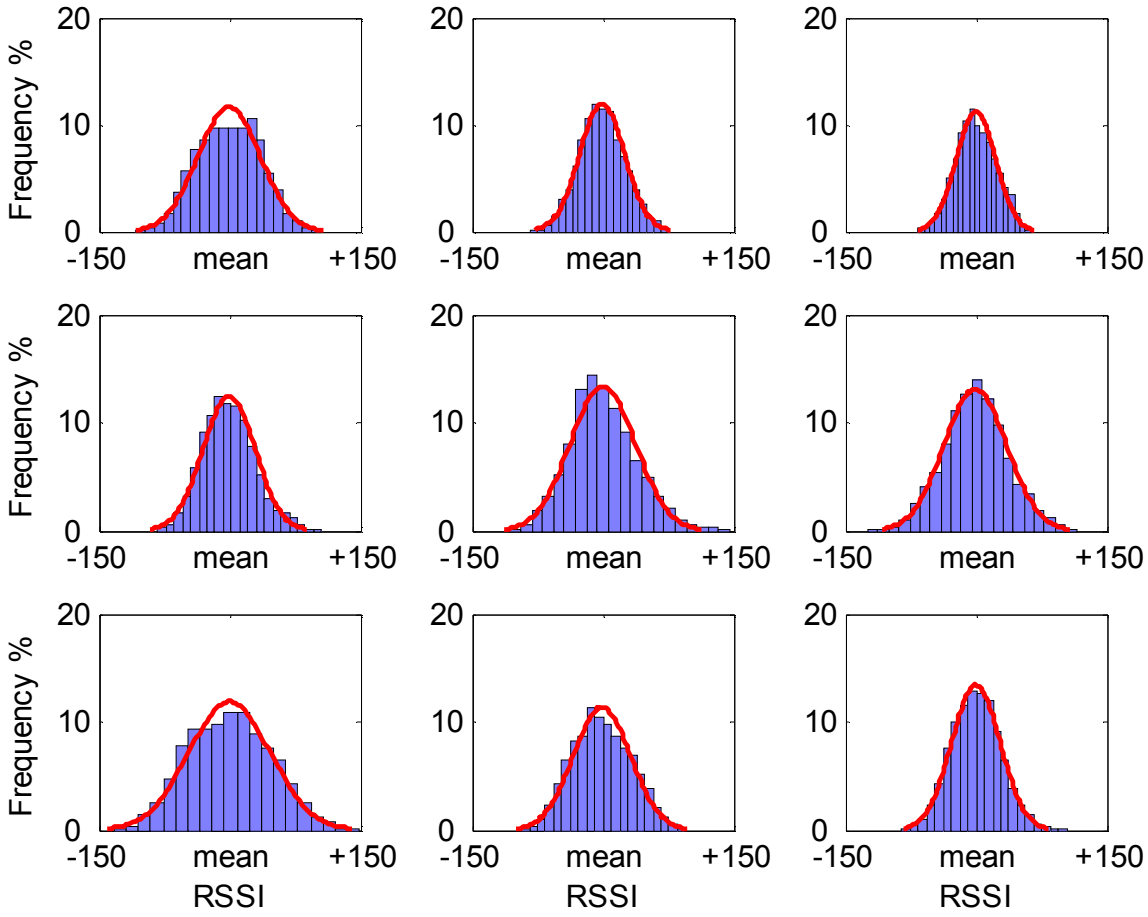

Figure 19. Processed RSSI distributions at the locations corresponding to those in Figure 17 using the preprocessor with N = 110. The bell curves are fitted Gaussian distributions.

4.5.5 RSSI Segmentation

Because an instant of RSSI is a random variable, to apply stochastic processes a certain period time of RSSI is required. There are two typical data segmentations, overlapping and non-overlapping. We use non-overlapping segments, "frames", (Figure 20) of processed RSSI as the observations to an HMM classifier, which makes decisions at each frame-time instant. Then, motion-transition finder searches within the selected frame for the exact time of transition from stationary to moving state. In contrast to frame-based segmentation, a sliding-window segmentation

Figure 21) can makes decisions at each sample time instant. It, however, shares most of the data within the adjacent windows and produces highly correlated information, making it difficult to detect the differences between two consecutive windows.

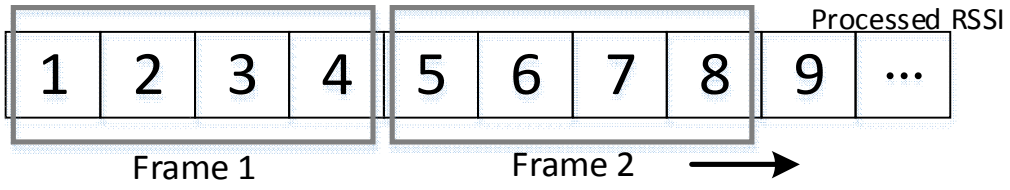

Figure 20. Frame based (non-overlapping) segmentation of time series data.

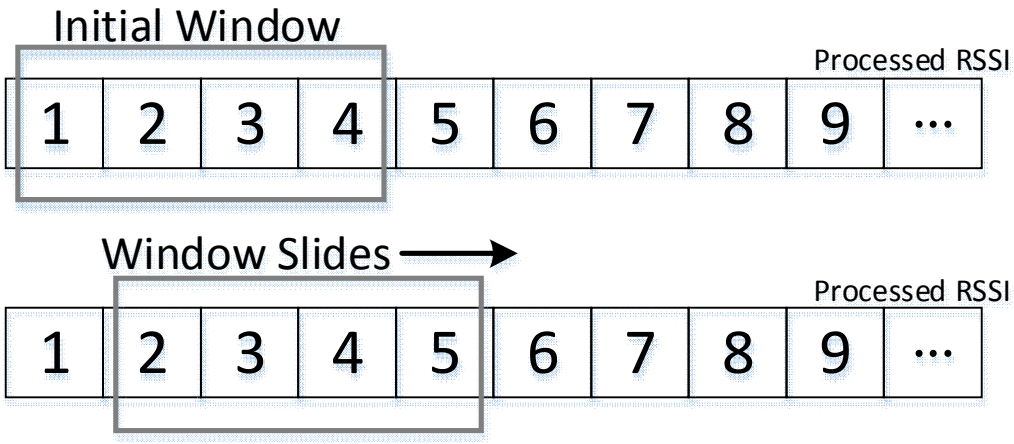

Figure 21. Sliding window (overlapping) based segmentation of time series data.

4.5.6 Transition Detection

The advantage of frame based segmentation is that consecutive data frames have no correlation introduced from the segmentation but the frame segmentation produces less accurate decision point in time than the sliding window. In the case of sliding window (Figure 21), data segmentations are generated at every instant of data and detection can be made at the same time. In the frame segmentation, data segmentations are generated at a multiple data instant period and detection cannot be made at a single instant data time. Thus we introduce a motion-transition finder to find the exact

detection time.

Each frame is fed to the HMM classifier as an observation and the HMM classifier marks each frame with either “moving” or “stationary” state. Then motion-transition finder searches for the exact start and end time of state transition. Figure 22 shows a set of frames used by motion-transition finder, with “stationary” frames and “moving” frames. We use two line segments for curve fitting, because in stationary states the processed RSSI can be fitted with a horizontal line, and in moving states after a stationary state it can be fitted with a linear line. The first segment is a horizontal line corresponding to the mean value of the first stationary frame. The segment after or before a stationary state is a linear line connecting the horizontal lines representing the moving states. The connecting pint of two fitted lines indicates the exact start and end times (in seconds) of the state transition (i.e., the beginning and the end of object movement).

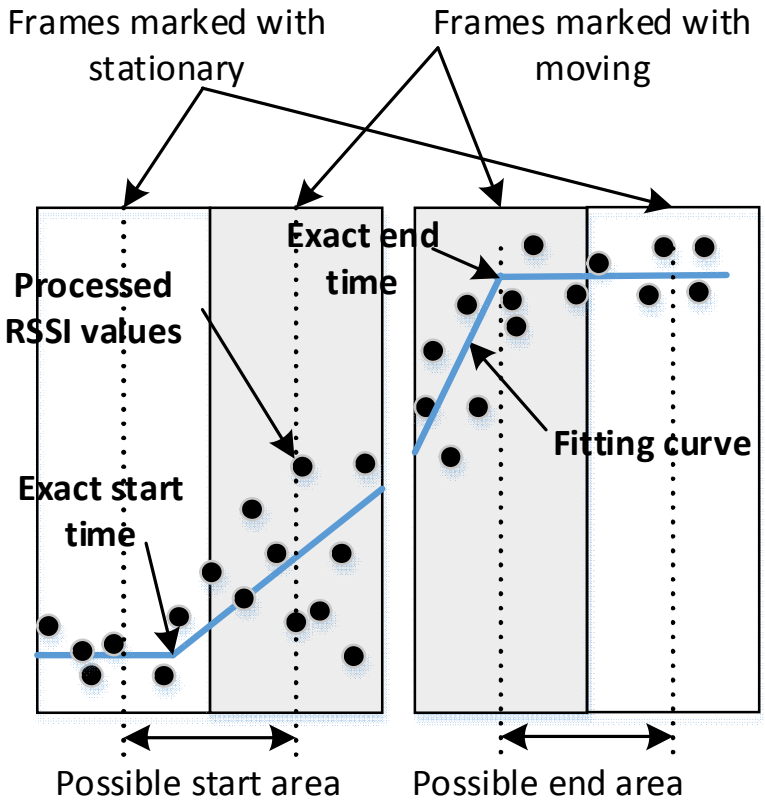

Figure 22. A set of frames for motion-transition finder and a fitting curve.

4.6 HMM Classifier

4.6.1 Naive Hidden Markov Model (NHMM)

We first designed a NHMM (Figure 23 (a)) that makes decisions whether the tagged object is moving or stationary and then introduced Augmented Hidden

Markov Model (AHMM) and Simplified AHMM (SAHMM). Given NHMM, the Viterbi Algorithm [74] is used to find the most likely state sequence through the trellis (Figure 23 (b)) by maximizing the probability of the most probable state sequence (Equation 12 - 14).

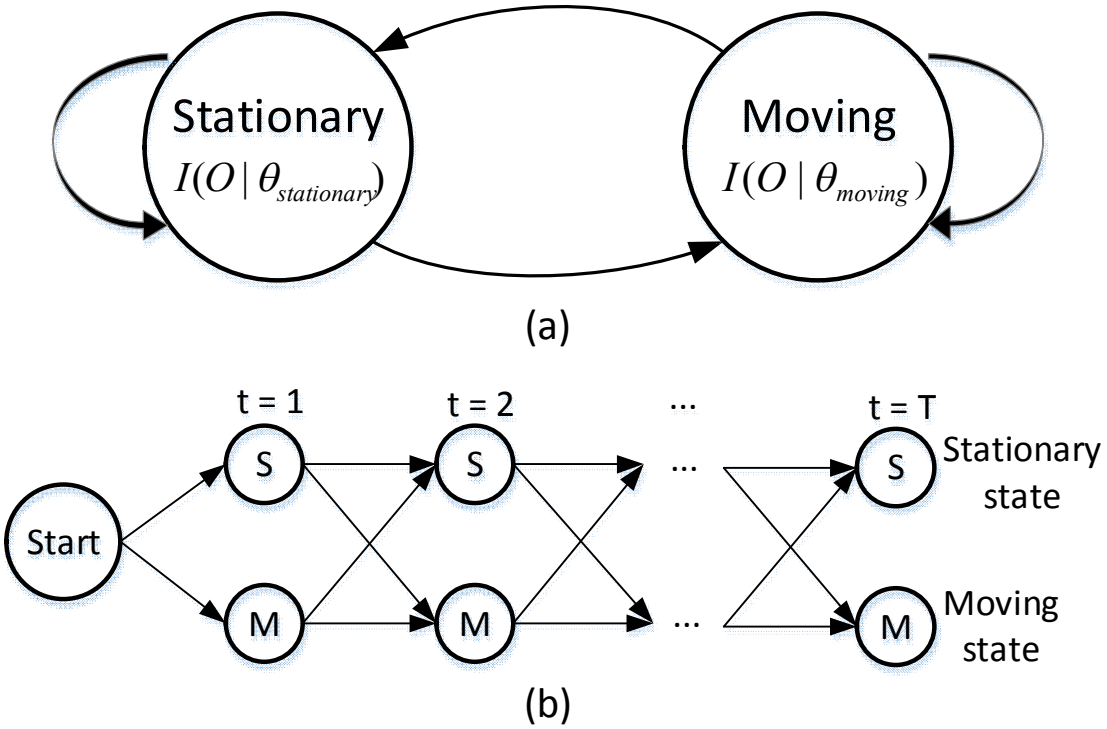

Figure 23. (a) State diagram of the Naive hidden Markov model; $I(x \mid \theta)$ is the emission probability distribution where o is the observation (Equation 15). (b) Trellis form the Viterbi Algorithm to compute the most-likely corresponding sequence of state.

$$v_\theta(1) = I(o_t \mid \theta) \cdot \pi_\theta \qquad \text{(Initial State)} \tag{12}$$

$$v_\theta(t) = v_\theta(t-1) \cdot I(o_t \mid \theta) \cdot a_{i,\theta} \tag{13}$$

$$q(t) = \arg\max_\theta v_\theta(t) \tag{14}$$

where $1 \le t \le T$, o_t = observation, θ, i = {stationary state, moving state}, π_θ = initial probabilities of θ, $a_{i,\theta}$ = probabilities of transitioning from i to θ, and the most likely state sequence = $q(t)$.

All the parameters of NHMM are defined and explained as follows.

Observations

Our system is based on RSSI which can vary with diversity of reader antenna gain and tag antenna gain associated with device hardware. Those devices' diversity causes additional magnitudes in RSSI measurement but the additional magnitudes are different with different tags and reader antennas. By subtracting RSSI values from the same tag on a frame basis, we eliminate the common additional magnitude of each frame RSSI introduced by the diversity. Because RSSI is provided in a logarithmic scale (dBm), the

additional magnitude is added to RSSI as a constant number. For instance, the difference of sample means of RSSI values from a stationary tag tends to be zero regardless of an extra magnitude in RSSI values from the device diversity. Thus, we define NHMM observations to be the difference between the mean RSSI values of the current frame and the predecessor frame:

$$o_t = m_t - m_{t-1}, \qquad t \geq 2 \tag{15}$$

where t is the frame based time and m_t is the mean of processed RSSI values in frame t.

The emission probabilities in the states

Processed RSSI is a Gaussian random variable and any liner transformation of processed RSSI produces another Gaussian random, variable. Thus m_t (μ_{m_t} , σ_{m_t}), m_{t-1} ($\mu_{m_{t-1}}$, $\sigma_{m_{t-1}}$) and O_t ($\mu_{o_t} = \mu_{m_t} - \mu_{m_{t-1}}$, $\sigma_{o_t} = \sigma_{m_t} + \sigma_{m_{t-1}}$) are Gaussian random variables (Equation 16)

$$P_{O_t}(x) = \frac{1}{2\pi\sigma_{m_n}\sigma_{m_{n-1}}} \int_{-\infty}^{\infty}\int_{-\infty}^{\infty} \exp\left(\frac{-x_n^2}{2\sigma_{m_n}^2}\right)\exp\left(\frac{-x_{n-1}^2}{2\sigma_{m_{n-1}}^2}\right)\delta((x_n - x_{n-1}) - x)dx_n dx_{n-1}$$

$$= \frac{1}{\sqrt{2\pi(\sigma_{m_n}^2 + \sigma_{m_{n-1}}^2)}} \exp\left(\frac{-[x - (\mu_{m_n} - \mu_{m_{x-1}})]^2}{2(\sigma_{m_n}^2 + \sigma_{m_{n-1}}^2)}\right) \tag{16}$$

where $\delta(x)$ is a delta function.

Because the probability distribution of the input function follows a Gaussian, it is possible to represent analytically the continuous observations for emission probabilities of an HMM as a Gaussian distribution. Using the Gaussian distribution of the observations the emission probabilities of observations in the stationary state and moving state are defined:

An emission probability of observation o_t in the stationary state defined as $I(o_t \mid \theta_{stationary})$ follows Gaussian ($\mu_{o_t} = 0$, $\sigma_{o_t} = \sigma_{m_t} + \sigma_{m_{t-1}}$). In the stationary state, μ_{o_t} is zero because of $\mu_{m_t} = \mu_{m_{t-1}}$.

An emission probability of observation o_t in the moving state defined as $I(o_t \mid \theta_{moving})$ follows Gaussian ($\mu_{o_t} = \mu_{m_t} - \mu_{m_{t-1}}$, $\sigma_{o_t} = \sigma_{m_t} + \sigma_{m_{t-1}}$).

The mean and standard deviation in each state are decided and optimized with training data sets.

Optimality criterion

The target to detect is whether an object moving. False positive error generates false information on the motion of moving while false negative error results in losing the motion information. Both types of errors should be minimized. In our context, sizes of the positive (moving) and negative (stationary) classes are different. The number of the stationary states overruns the number of the moving states since objects are more likely in stationary. We use Matthew's Correlation Coefficient (MCC) [75] (Equation 17 - 20) as an optimality criterion for our HMM classifier because it works with skewed class imbalance and takes into account both false positive and false negative errors [76].

$$N = TN + TP + FN + FP \tag{17}$$

$$S = \frac{TP + FN}{N} \tag{18}$$

$$P = \frac{TP + FP}{N} \tag{19}$$

$$MCC = \frac{\frac{TP}{N} - S \times P}{\sqrt{PS\,(1-s)(1-P)}} \tag{20}$$

Where TP is the number of true positives, TN is the number of true negatives, FP is the number of false positives and FN is the number of false negatives.

Initial and transition probabilities

By supervised training, initial and transition probabilities are learned from respective frequencies of state transitions from training data sets.

4.6.2 Augmented Hidden Markov Model (AHMM)

With the property that reducing the variance of a RSSI distribution contributes to lowering the overlapping area of distributions of different RSSI sets which results in errors (Figure 18), we design AHMM (Figure 24) to reduce the variance of the observation (Equation 16) in the stationary states. In a period of frames in which the stationary state keeps continuing, each mean of the frame data converges the mean of the period data and m_{t-1} can be replaced with $\hat{m}_{t-1}$. The observation of continuing stationary states is:

$$o_t = m_t - \hat{m}_{t-1} \tag{21}$$

$$\hat{m}_{t-1} = \frac{1}{k}\sum_{i=0}^{k-1} m_{(t-1)-i} \tag{22}$$

where k is the number of continuing stationary states.

By processing multiple stationary frames, the variance of averaged $\hat{m}_{t-1}$ is reduced, so the observation variance in continuing stationary states, $\sigma_{o_t}^2 (= \sigma_{m_t}^2 + \sigma_{\hat{m}_{t-1}}^2)$ becomes smaller than the observation distribution in Equation 16. By the CLT, upon further increasing k, $\sigma_{\hat{m}_{t-1}}^2$ converges zero, so the observation distribution in continuing stationary states can be reduced to $\sigma_{m_t}^2$. Figure 25 shows an experimental result. The stationary state continues, on average, variances of $\hat{m}_{t-1}$ are reducing quickly below $0.15 \times \sigma_{m_{t-1}}^2$ at 8th continuing stationary state. The used RSSI values are taken ten thousand times from a stationary tag at the nine locations (Figure 17). Figure 24 shows the states of AHMM to reduce the observation variance in the stationary states. In each stationary state, $\hat{m}_{t-1}$ is updated using Equation 22 and results in reduced variances of the observation.

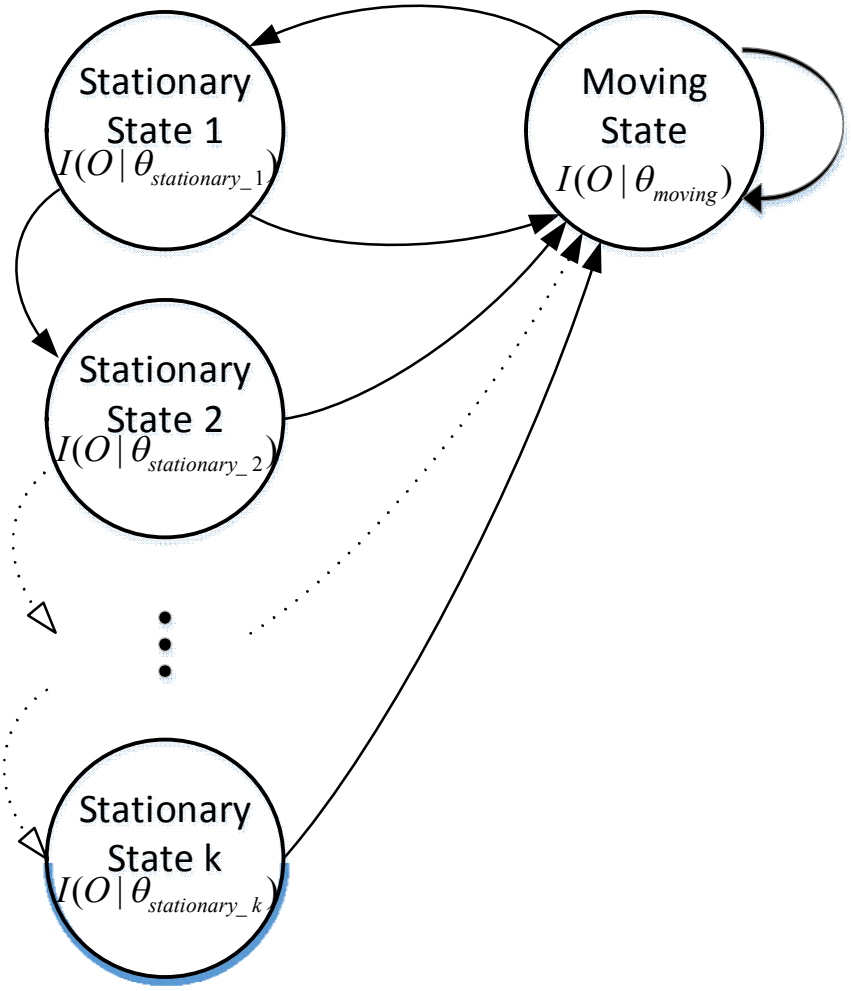

Figure 24. The state diagram of AHMM.

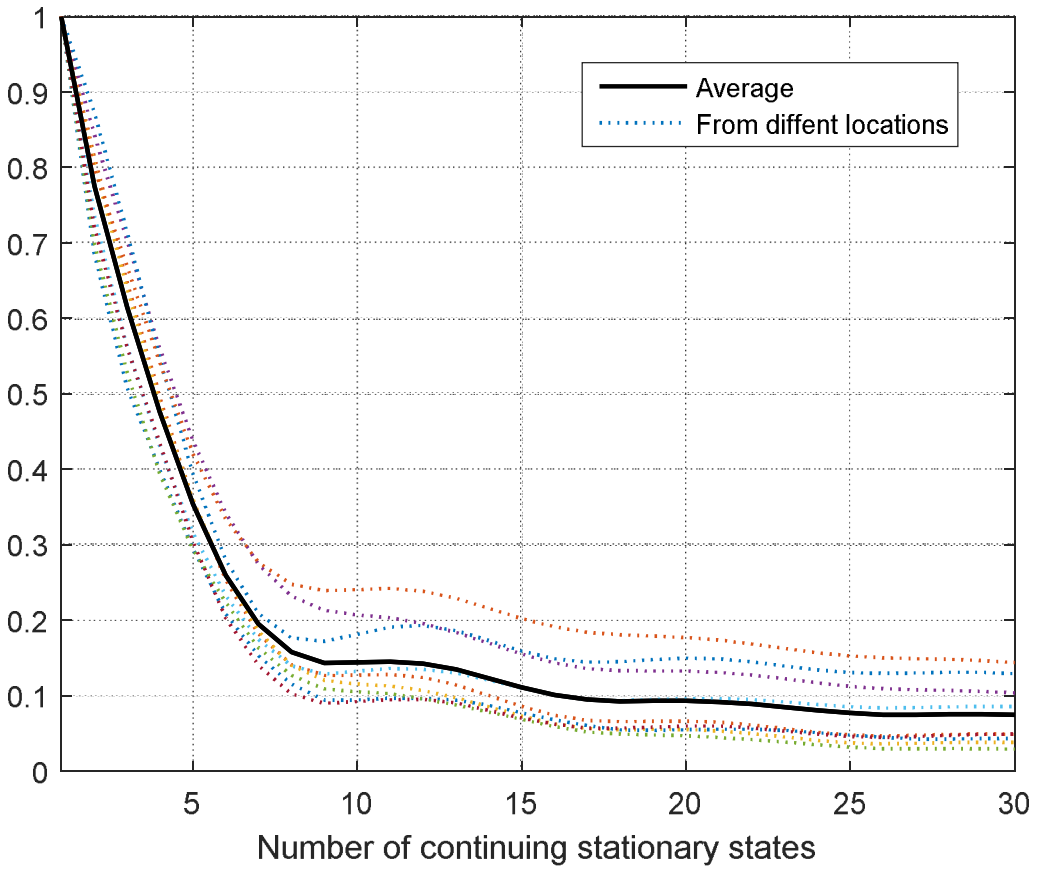

Figure 25. The ratio of variance of $\hat{m}_{t-1}$ to m_{t-1} as the stationary state continues. RSSI data are taken at the same nine locations as in Figure 17.

4.6.3 Simplified AHMM (SAHMM)

The critical impediment in realization of AHMM is to train a number of states since supervised training is used in our context. To yield stable

parameters of all the fine stationary states, the training requires much more training data and ground truths involving a great amount of fine handwork. Thus, we simplify a number of the stationary states of AHMM to a single stationary state for feasible training while keep the property of reducing the observation distribution. Thus SAHMM has one stationary state and one moving state as in NHMM but uses the same observations of AHMM.

Observations

We use the observations to AHMM defined in Equation 21 and 22 from the previous section. As the stationary state continues, $\hat{m}_{t-1}$ can be determined with m_{t-1} and $\hat{m}_{t-2}$, that is from the previous stationary state, without using all the history of m:

$$\hat{m}_{t-1} = (\hat{m}_{t-2} \times (k-1) + m_{n-1}) / k \tag{23}$$

where k is the number of continuing stationary states (Figure 24).

Thus the observation to SHMM can be realized in a functional form with m_t, m_{t-1} and $\hat{m}_{t-2}$ without using additional memories and further history of data.

Emission probabilities of the states

Emission probabilities $I(O|\theta_{moving})$ and $I(O|\theta_{stationary})$ remain unchanged as in AHMM, while with training data sets, the variance of the emission probabilities is trained.

Initial and transition probability distributions

By supervised training, those distributions also remain unchanged as in NHMM.

5. System Evaluation

5.1 Individual Component Evaluation

In this section, we show how each component of the detection system works with three experimental scenarios (Figure 26 – Figure 28). Those scenarios consist of the cases of four people moving around, one person moving and monotonous increment of RSSI with respect to human interference and detectable RSSI changes. Our area of interest is the patient bed in a trauma resuscitation room, surrounded by a medical team treating the patient

(Figure 11). In the scenario of four people moving around the bed, much bigger ripples in stationary-state RSSI values were observed compared to the scenario with one person moving (Figure 27). NHMM and SAHMM were trained using a set of RSSI values from the first scenario (Figure 26), and applied to all three scenarios. Because of the training set with heavy ripples, both SAHMM and NHMM might miss small changes in RSSI value (Figure 28). Due to the reducing-variance characteristics of SAHMM, it detects all the movements in Figure 26 except for the smallest movements (Figure 28). NHMM, however, misses most of the smallest changes (Figure 28).

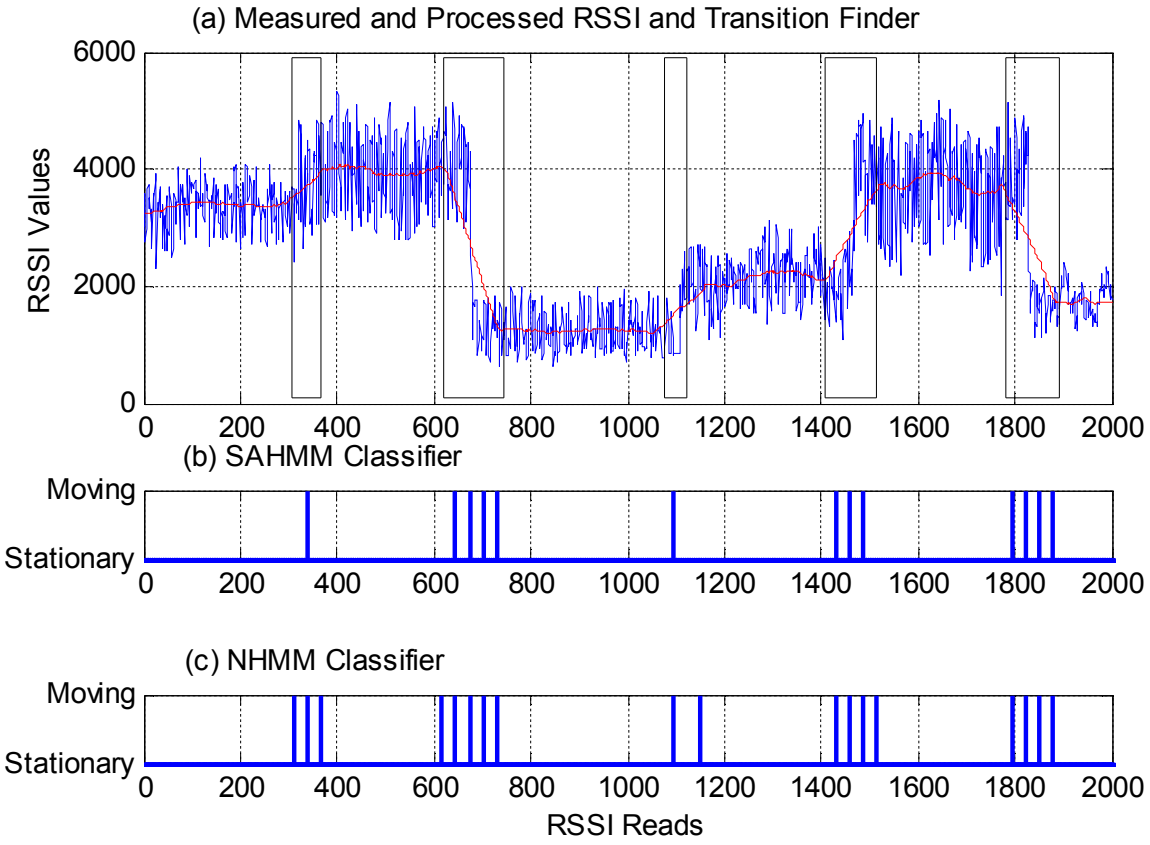

Figure 26. A scenario with random tag movement and four people moving randomly in the area of interest, (a) Spiky lines show measured RSSI values, the smooth line shows processed RSSI, and rectangular boxes show the exact transition times from motion-transition finder with SAHMM outputs; (b) Detection output of ASHMM; (c) Detection output of NHMM at each frame instant.

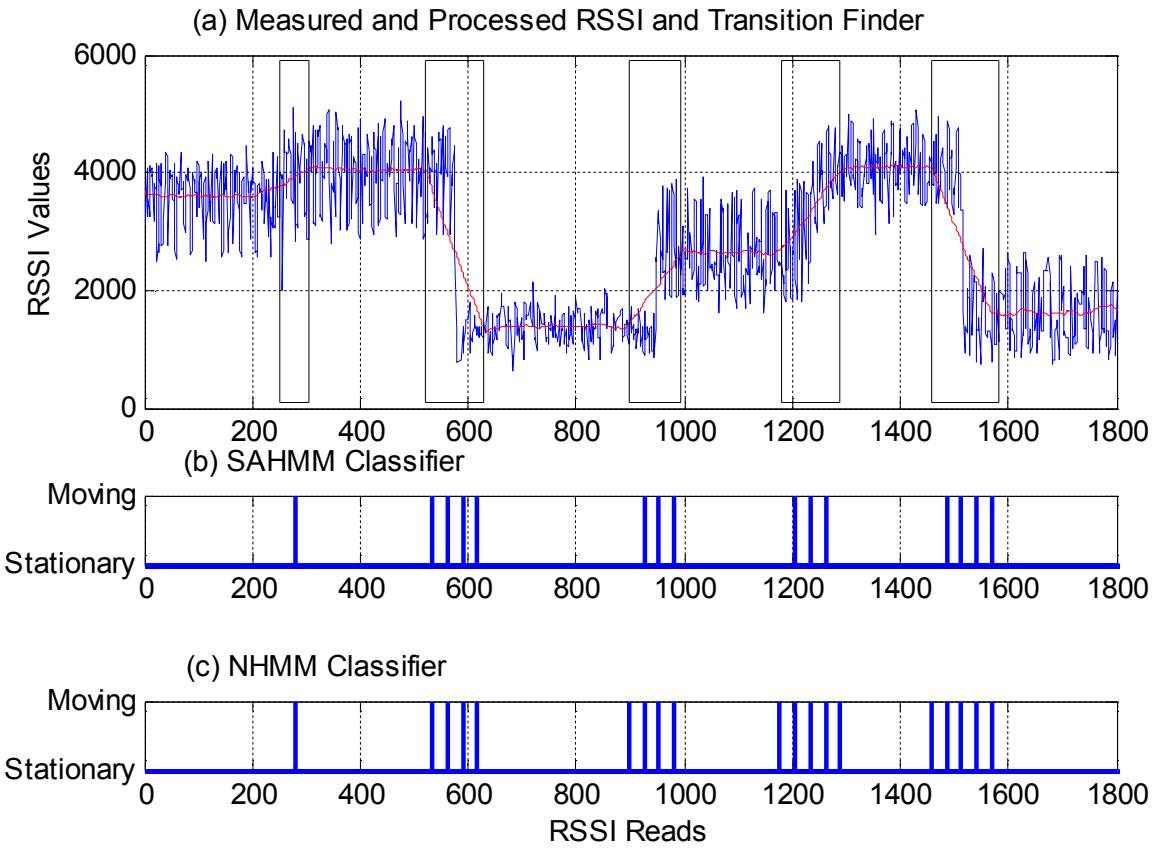

Figure 27. A scenario with random tag movement and one person moving in the area of interest. Charts (a) – (c) have the same meaning as in Figure 26.

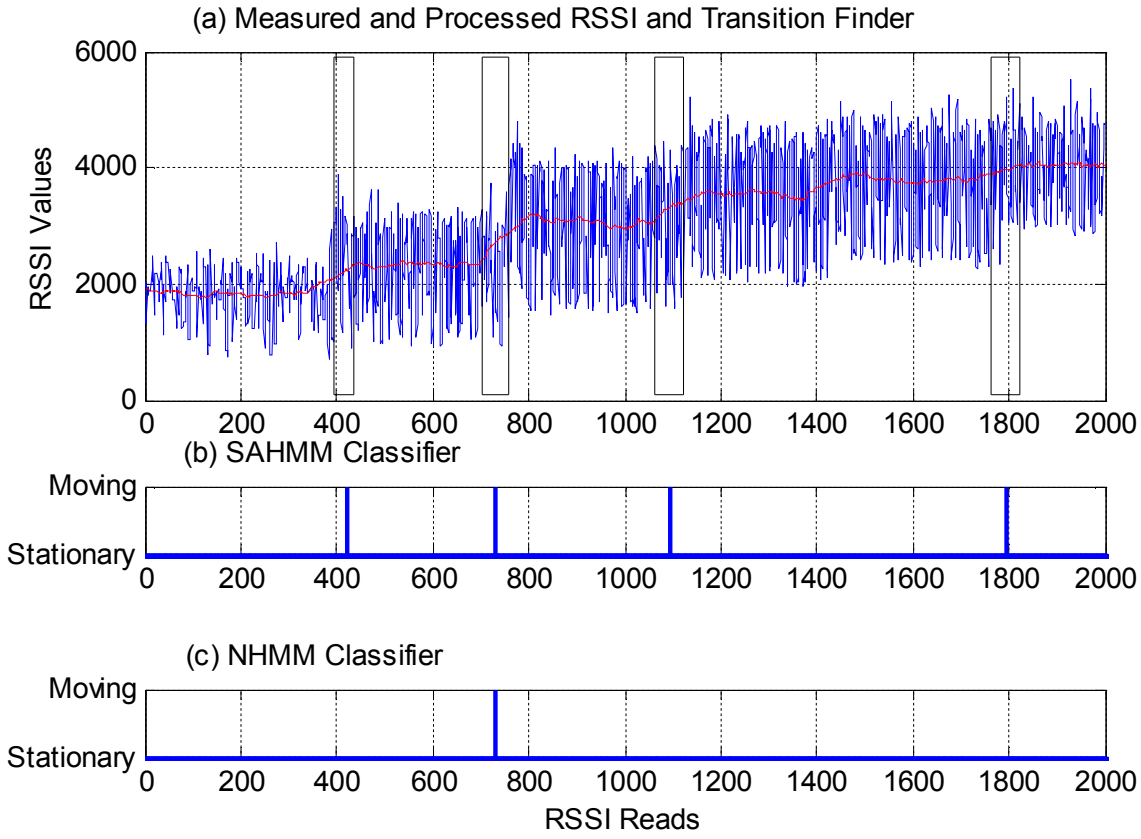

Figure 28. A scenario with the tag's rotating to produce small RSSI increments in monotone and one person moving in the area of interest. Charts (a) – (c) have the same meaning as in Figure 26.

5.2 System Hardware

We used and installed UHF RFID equipment from Alien Technology [43] and Confidex which includes two of RFID reader ALR-9900, four circularly polarized wide angle antenna ALR-8696-C and two types of passive UHF tags (ALN-9740 and Confidex Steelwave Micro II [77]). The four reader antennas

point to the patient bed from different viewing angles. These antennas allow to integrate tags at all directions and also produce RSSI in any cases that medical staffs might obscure one of the antennas' line-of-sight RFID signals resulting in degrading signal strength and an insufficient data set in number. The RFID readers and a desktop computer are connected to a router for TCP/IP communication. The reader has a local clock and offers a timestamp in a millisecond resolution for each RSSI read. The timestamp is used for the fixed frame in time. Two different types of passive UHF tags are used for different materials of medical objects. One type is ALN-9740 for non-metallic objects, its dimensions are 98.2×12.3×0.08 mm and the read range is up to 12 m. The other type is Confidex Steelwave Micro II for metallic objects such as laryngoscope and its dimensions and read range are 38×13×4.5 mm and up to 5 m on metal. The communication protocol used between the readers and the passive tags is the EPC ClASS-1 Generation-2 standard.

5.3 Tagged Passive Medical Objects

Nine passive medical objects are selected and tagged, mostly used on and near to the patient bed in resuscitations such as bag valve mask (BVM), collar, laryngoscope, ETtube (ETT), Stethoscope, Fluid bag, IV start kit, IV

tubing, and thermometer (Figure 29).

Figure 29. The tagged passive medical objects; from upper left, ETT, IV start kit, thermometer and stethoscope. From lower left, laryngoscope, collar, IV tubing, fluid bag and BVM.

5.4 Data Collection and Ground Truth Data

With the deployment of the RFID system, RFID data and surveillance video are recorded during 28 simulated resuscitations, each about 20 minutes long. The recorded surveillance videos are used to make ground truth data. There are four resuscitation scenarios and each one was preformed seven times by different trauma teams. The average number of medical staffs moving around

the area of interest is four in the resuscitations. The scenarios include High-speed motor vehicle collision, pedestrian struck at approx 20 mph, restrained passenger in head-on collision and pedestrian struck in a parking lot, involving the nine passive medical objects for treatments such as endotracheal intubation, administration of fluids and mediations, temperature control and ET-tube insertion.

5.5 Experimental Results

From the 28 resuscitations, 20 resuscitations, each five resuscitations from four different scenarios, are taken at random and used for training NHMM and SAHMM and eight resuscitations are used for evaluations. The results are shown in Figure 30. Each of tagged objects has distinctive usage and moving characteristic so detection accuracies are slightly different. RSSI data are extracted according to tag's ID and the antenna and feed to the detection system with distinct parameters. Data from different antennas might produce contrastive detections. Then the detection with a higher data rate is taken because better signal reception results in higher data rates.

SAHMM shows 10.8% improvement in accuracy on average compared to

NHMM. The object movement is identified with 89.5% accuracy on average by SAHMM. The stethoscope shows the lowest accuracy of 72.4% from the fact that most radio signals from the tag are absorbed by human body resulting in low data rates. In general, medical staffs carry stethoscopes on the chest or around the neck when not in-use so human body can absorbs both signals from a reader antenna and backscattered signals from a tag attached on the stethoscope. This absorbing effect results in missing RSSI reads and a low accuracy.

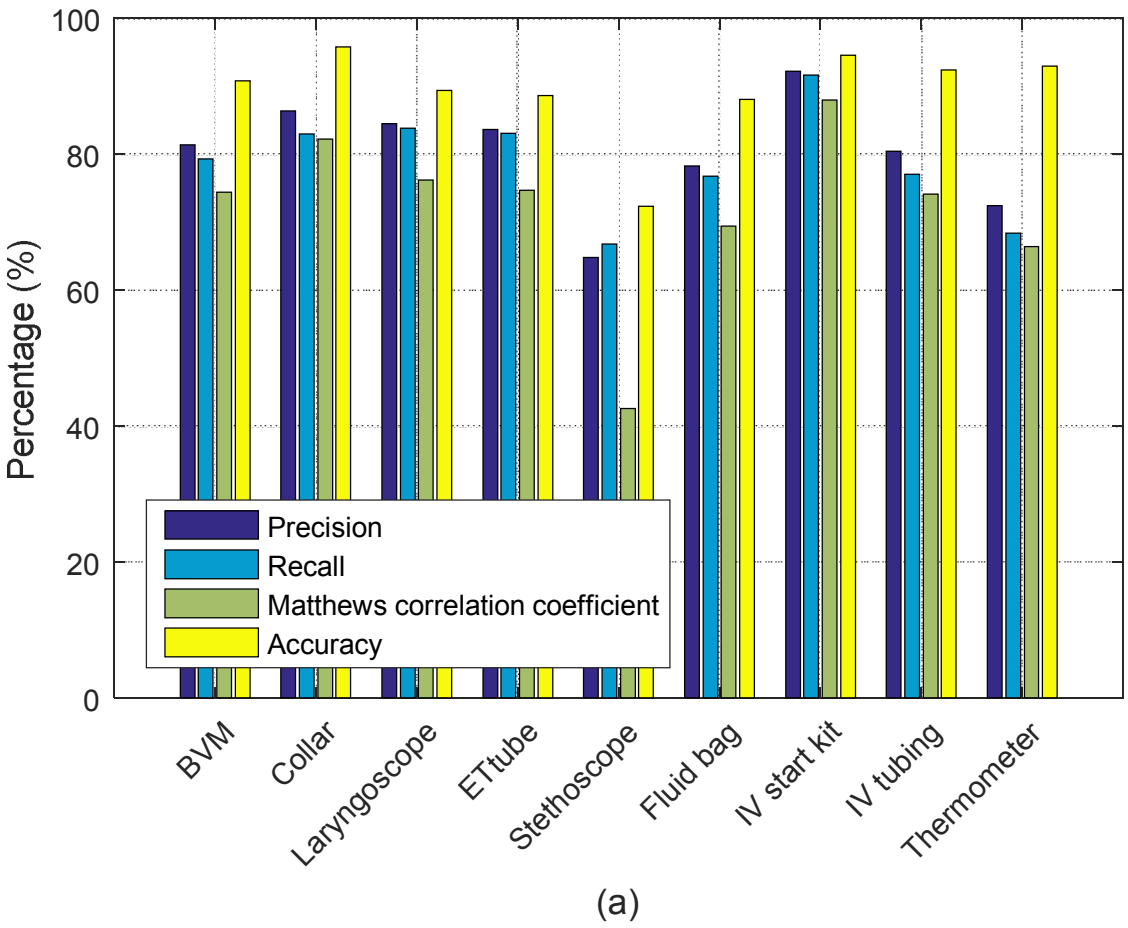
100
80
60
40
20
0
Percentage (%)
Precision
Recall
Matthews correlation coefficient
Accuracy
BVM
Collar
Laryngoscope
ETtube
Stethoscope
Fluid bag
IV start kit
IV tubing
Thermometer

(a)

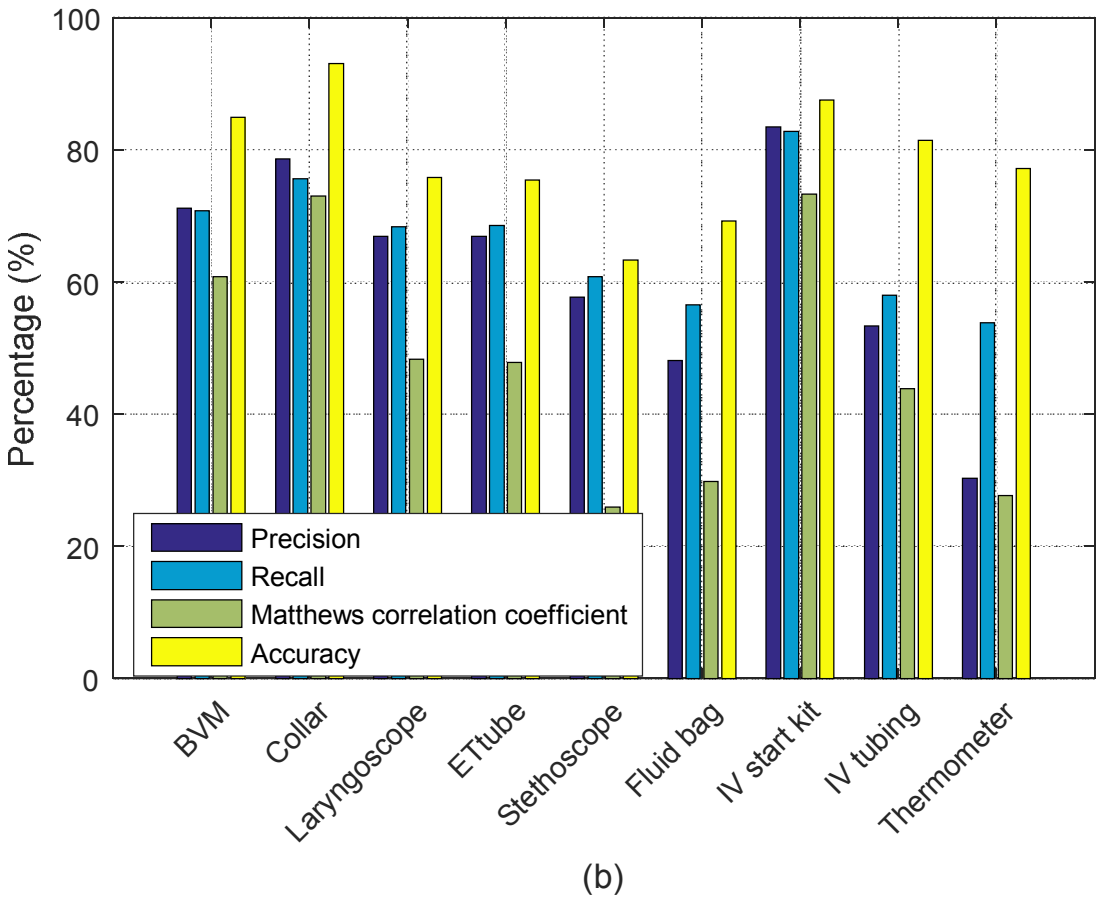

Figure 30. Motion detection performance of classifiers. (a) Results from SAHMM. (b) Results from NHMM.

6. Conclusion

Applications of UHF RFID passive tags have expanded from simply indentifying objects to tracking objects in various work and home settings. However, uninformed configurations of reader antennas may experience

power loss at tags even within their coverage area, rendering them inadequate for continuous tracking of tags. We identified the causes of the power loss as breakpoints and antennas angle mismatch between the reader and a randomly oriented tag. Breakpoints are created from indoor radio signal propagation and cannot be avoided. We presented a UHF RFID sensing platform that addresses the power loss problems using angle and spatial diversity. Our design provides uninterrupted coverage of the area of interest, eliminating the power loss problems and allowing continuous tracking of tags. We applied this sensing platform in a hospital trauma bay. We measured RSSI and query response rates for breakpoints and angle mismatch, and found no points with significant power loss. We conclude that this sensing platform provides uninterrupted tracking of RFID-tagged objects in indoor settings.

Having the sensor platform designed we present a detection system for providing information on moving and stationary motion of passive medical objects being used in the area of interest using UHF RFID technology. The novel methods to achieve a high accuracy are RSSI preprocessor, SAHMM classifier, frame based segmentation and motion-transition finder. The RSSI preprocessor reduces the variance of RSSI distribution introduced by the thermal noise and makes accurate approximations to the Gaussian

distribution. To detect tagged object's motion, we use RSSI change of the tag based on its relocation with frame based segmentation of RSSI data. The motion-transition finder determines the exact movement time within a frame based period. SAHMM is trained for crowded settings with human moving and the movement and in-use frequency of each tagged object to maximize its detection accuracy tackling environmental interference. Proposed SAHMM increases the detection accuracy by 10.8% compared to NHMM. Our system is evaluated with RSSI data recorded in an actual trauma bay in simulated resuscitations performed by trauma teams and shows 89.5% accuracy with human moving around the area of interest. From this result we expect that passive UHF RFID technology can be a promising method to provide information on both the movement and identification of passive medical objects for context-aware systems.

References

[1] Levine W., Meyer M., Brzezinski P., Robbins J., and Sandberg W., "Computer Automated Total Perioperative," Computer Assisted Radiology and Surgery, 2005.

[2] Satava R., "Telesurgery, robotics, and the future of telemedicine," European Surgery, 37(5):304–307, 2005.

[3] Bardram J. E., "Applications of Context-Aware Computing in HospitalWork Examples and Design Principles," In Proceedings of the 2004 ACM Symposium on Applied Computing, 2004.

[4] H. Lehpamer, "RFID Design Principles," Artech House, Inc., 2008.

[5] A. Cangialosi, J. Monaly, and S. Yang, "Leveraging RFID in Hospitals: Patient Life Cycle and Mobility Perspectives," IEEE Communications Magazine, vol. 45, no. 9, pp. 18–23, September 2007.

[6] L. Boglione, "RFID technology - are you ready for it?," IEEE Microwave Magazine, vol. 8, no. 6, pp. 30 – 32, Dec. 2007.

[7] D. Dobkin and T. Wandinger, "A radio-oriented introduction to RFID," High Frequency Electronics, pp. 46-54, June 2005.

[8] S. Agarwal, A. Joshi, T. Finin, Y. Yesha, and T. Ganous, "A pervasive computing system for the operating room of the future," Mobile Networks and Applications, vol. 12, no. 2-3, pp. 215-228, 2007.

[9] S.R. Banerjee, R. Jesme, and R.A. Sainati, "Performance analysis of short range UHF propagation as applicable to passive RFID," in Proc. IEEE RFID Conference, pp. 30-36, 2007.

[10] S. Parlak, A. Sarcevic, I. Marsic and R. S. Burd, "Introducing RFID technology in dynamic and time-critical settings: Requirements and challenges," Journal of Biomedical Informatics, vol. 45, no. 5, pp. 958-974, 2012.

[11] D. Joho, C. Plagemann, and W. Burgard, "Modeling RFID signal strength and tag detection for localization and mapping," in Proc. IEEE Int'l Conf. Robotics and Automation, pp.3160-3165, 2009.

[12] J. Torres-Solis, T.H. Falk, and T. Chau, "A review of indoor localization technologies: towards navigational assistance for topographical disorientation," Ambient Intelligence, pp.51-84, 2010.

[13] J.E. Bardram, A. Doryab, R. M. Jensen, P.M. Lange, K.L. Nielsen, and S.T. Petersen, "Phase recognition during surgical procedures using embedded and body-worn sensors," In Pervasive Computing and Communications (PerCom), IEEE International Conference on, pp. 45-53, 2011, March.

[14] T. Inomata, F. Naya, N. Kuwahara, F. Hattori, and K. Kogure, "Activity recognition from interactions with objects using dynamic bayesian network," In Proceedings of the 3rd ACM International Workshop on Context-Awareness for Self-Managing Systems, pp. 39-42, 2009, May.

[15] B. Logan, J. Healey, M. Philipose, E. Tapia, and S. Intille, "A long-term evaluation of sensing modalities for activity recognition," Springer Berlin Heidelberg, pp. 483-500, 2007.

[16] K. Ohashi, S. Ota, L. Ohno-Machado, and H. Tanaka, "Smart medical environment at the point of care: Auto-tracking clinical interventions at the bed side using RFID technology," Computers in Biology and Medicine, vol. 40, no. 6, pp. 545-554, 2010.

[17] M. Buettner, R. Prasad, M. Philipose, and D. Wetherall, "Recognizing daily activities with RFID-based sensors," In Proceedings of the 11th international conference on Ubiquitous computing, pp. 51-60. ACM, 2009.

[18] D. Kim, M.A. Ingram, and W.W. Smith, "Measurements of small-scale fading and path loss for long range RF tags," IEEE transactions on Antennas and Propagation, vol.51, no.8, pp.1740-1749, Nov 2003.

[19] L.W. Mayer, M. Wrulich, and S. Caban, "Measurements and channel modeling for short range indoor UHF applications," Proceedings of The European Conference on Antennas and Propagation, 2006.

[20] S. Preradovic and N. Karmakar, "RFID readers - a review," International Conference on Elec. and Comp. Eng., pp. 100-103, Dec. 2006.

[21] M. Reynolds and C. Weigand, "Design considerations for embedded software-defined RFID readers," Emerging Technology, pp. 14-15, August 2005.

[22] S. Parlak and I. Marsic, "Detecting object motion using passive RFID: A trauma resuscitation case study," IEEE Trans. Instrum. Meas., vol.62, no.9, pp.2430-2437, Sept 2013.

[23] S. Parlak, S. Ayyer, Y. Y. Liu, and I. Marsic, " Design and Evaluation of RFID Deployments in a Trauma Resuscitation Bay," Biomedical and Health Informatics, IEEE Journal of, vol. 18, no. 3, pp. 1091-1097, 2014.

[24] A. Chattopadhyay and A. Harish, "Analysis of low range indoor location tracking techniques using passive UHF RFID tags," Proc. 2008 IEEE Radio and Wireless Symposium, pp. 351-354, January 2008.

[25] P.V. Nikitin and K.V.S. Rao, "Antennas and propagation in UHF RFID systems," in Proc. IEEE Int'l Conf. RFID, Las Vegas, NV, pp. 277-288, 2008.

[26] J.S. Choi, H. Lee, R. Elmasri and D.W. Engels, "Localization systems using passive UHF RFID," Proc. Fifth International Joint Conference on INC, IMS and IDC, pp.1727-1732, August 2009.

[27] A. Nemmaluri, M.D. Corner, and P. Shenoy, "Sherlock: Automatically locating objects for humans," Proc. ACM MobiSys pp.187-198, 2008.

[28] S.C.M Perera, A.G. Wiliamson and G.B. Rowe, "Prediction of breakpoint distance in microcellular environments," Electronics Letters, vol.35, no.14, pp.1135-1136, July 1999.

[29] B. Jiang, K. P. Fishkin, S. Roy, and M. Philipose, "Unobtrusive long-range detection of passive RFID tag motion," Instrumentation and Measurement, IEEE Transactions on, vol. 55, no. 1, pp. 187-196, 2006.

[30] S. Zhou and J. Pollard, "Position Measurement Using Bluetooth," IEEE Transactions on Consumer Electronics, vol. 52, no. 2, pp. 555–558, May 2006.

[31] Y. Chen and H. Kobayashi, "Signal Strength Based Indoor Geolocation," IEEE International Conference on Communications, vol. 1, pp. 436–439, 2002.

[32] R. Akl, D. Tummala, and X. Li, "Indoor Propagation Modelinlg at 2.4 GHZ for IEEE 802.11 Networks," Wireless Networks and Emerging Technologies, July 2006.

[33] J. L. Brchan, L. Zhao, J. Wu, R. E. Williams, and L. C. Pérez, "A real-time RFID localization experiment using propagation models," Proc. 2012 IEEE International Conference on RFID, pp. 141-148, 2012.

[34] Azadeh Kushki, Konstantinos N. Plataniotis, and Anastasios N. Venetsanopoulos, " Kernel-based positioning in wireless local area networks," IEEE Transactions on Mobile Computing, v 6, n 6, p 689-705,

June, 2007.

[35] K. Pahlavan, Xinrong Li, and J. P. Makela, "Indoor geolocation science and technology," Communications Magazine, IEEE, 40(2):112-118, 2002.

[36] S. Roehr, P. Gulden, and M. Vossiek. Precise, "Distance and velocity measurement for realtime locating in multipath environments using a frequency-modulated continuous-wave secondary radar approach," IEEE Transactions on Microwave Theory and Techniques, 56(10):2329 - 2339, 2008.

[37] S. Venkatesh and R.M. Buehrer, "Non-line-of-sight identification in ultra-wideband systems based on received signal statistics," IET Microwaves, Antennas and Propagation 1(6):1120- 1130, 2007.

[38] Z. Zhang, C.L. Law, and E. Gunawan, "Multipath mitigation technique based on partial autocorrelation function," Wireless Personal Communications, v 41, n 1, p145-154, 2007.

[39] L. Yang, Y. Chen, X. Y. Li, C. Xiao, M. Li, and Y. Liu, "Tagoram: real-time tracking of mobile RFID tags to high precision using COTS devices," In Proceedings of the 20th annual international conference on Mobile computing and networking, pp. 237-248, ACM, 2014.

[40] P. Zhang, J. Gummeson, and D. Ganesan , "Blink: A high throughput link layer for backscatter communication," Proceedings of the 10th international conference on Mobile systems, applications, and services, ACM, pp. 99-112, 2012.

[41] L. W. Mayer, M. Wrulich, and S. Caban, "Measurements and channel modeling for short range indoor UHF applications," In Antennas and Propagation, 2006. EuCAP 2006. First European Conference on, pp. 1-5. IEEE, 2006.

[42] D. Dobkin, "Indoor propagation issues for wireless LANs," RF Design, pp 40-46, September 2000.

[43] "Alien Technology", online at http://www.alientechnology.com/.

[44] K. Finkenzeller, RFID Handbook, 3rd ed., : A John Wiley and Sons, Ltd., Publicaion, 2010, pp. 76-83..

[45] R. Poppe, " A survey on vision-based human action recognition," Image and vision computing, vol. 28, no. 6 pp. 976-990, 2010.

[46] D. Weinland, R. Ronfard, and E. Boyer, "A survey of vision-based methods for action representation, segmentation and recognition,"

Computer Vision and Image Understanding, vol.115, no.2, pp.224-241, 2011.

[47] A. M. Khan, Y. K. Lee, S. Y. Lee, and T. S. Kim, "A triaxial accelerometer-based physical-activity recognition via augmented-signal features and a hierarchical recognizer," Information Technology in Biomedicine, IEEE Transactions on, vol. 14 no. 5, pp. 1166-1172, 2010.

[48] "IMPINJ", online at www.impinj.com/about-rfid/types-of-rfid-systems/.

[49] B. Lee and B. Yu, "Compact structure of UHF band RFID tag antenna mounted on metallic objects," Microw. Opt. Technol. Lett., vol. 50, no.1, pp. 232–234, 2008.

[50] K. H. Lin, S. L. Chen, and R. Mittra, "A capacitively coupling multifeed slot antenna for metallic RFID tag design," IEEE Antennas Wireless Propag. Lett., vol. 9, pp. 447–450, 2010.

[51] S. Genovesi and A. Monorchio, "Low-profile three-arm folded dipole antenna for UHF band RFIDtags mountable onmetallic objects," IEEE Antennas Wireless Propag. Lett., vol. 9, pp. 1225–1228, 2011.

[52] P. H. Yang, Y. Li, L. Jiang, W. C. Chew, and T. T. Ye, "Compact metallic RFID tag antennas with a loop-fed method," IEEE Trans. Antennas and Propag., vol. 59, no. 12, pp. 4454–4462, 2011.

[53] B. D. Braaten, G. J. Owen, D. Vaselaar, and R. M. Nelson, "A printed rampart-line antenna with a dielectric superstrate for UHF RFID applications," in IEEE International Conference on RFID, pp. 74–80, 2008.

[54] R. Kanan and A. Azizi, "UHF RFID transponders antenna design for metal and wood surfaces," in IEEE International Conference on RFID, pp. 270–277, 2009.

[55] "RFID JPURNAL", online at www.rfidjournal.com/faq/show?68.

[56] S. Parlak, S. Ayyer, Y. Y. Liu, and I. Marsic, "Design and Evaluation of RFID Deployments in a Trauma Resuscitation Bay," Biomedical and Health Informatics, IEEE Journal of, vol. 18, no. 3, pp. 1091-1097, 2014.

[57] J. Jung et al., "Directional coupler for UHF mobile RFID reader," Microwave and Optical Technology Letters, vol. 49, no. 7, pp. 1501-1504, April 2007.

[58] H. Son et al., "Design of compact RFID reader antenna with high transmit/receive isolation," Microwave and Optical technology Letters,

vol. 48, no. 12, pp 2478-2481, December 2006.

[59] W. Kim et al., "A passive circulator with high isolation using a directional coupler for RFID," IEEE Microwave Symposium Digest pp. 1177 – 1180, June 2006.

[60] P. V. Nikitin and K. V. S. Rao, "Performance limitations of passive UHF RFID systems," IEEE Antennas and Propagation Symposium pp. 1011-1014, 2006.

[61] S. R. Banerjee, R. Jesme, and R. A. Sainati, "Performance analysis of short range UHF propagation as applicable to passive RFID," IEEE RFID Conference, pp. 30-36, 2007.

[62] T. Chau, B. Welt, W. Eisentadt, "Analysis and characterization of transponder antennae for RFID systems," Packaging Technology and Science, vol. 19, no. 1, pp. 33 – 44, 2006.

[63] S.Y. Tan and H.S. Tan, "Improved three dimensional ray tracing technique for microcellular propagation models," Electronics Letters, vol.31, no.17, pp.1503-1505, 17th, August 1995.

[64] A.J. Rustako, Jr., N. Amitay, G.J. Owens and R.S. Roman, "Radio propagation at microwave frequencies for line-of-sight microcellular mobile and personal communications," IEEE Trans. on Vehi. Tech., vol.40, no.1, pp.203-210, Feb 1991.

[65] Federal Communications Commission, online at http:// www.fcc.gov.

[66] D.M. Dobkin, "Tutorial: Radio Basics for UHF RFID," EE Times, July 2008.

[67] Wikipedia page on tiling by regular polygons: http://en.wikipedia.org/wiki/Tiling_by_regular_polygons.

[68] EPC/RFID Standards, online at: http://www.gs1.org/epc-rfid.

[69] P. Turaga, R. Chellappa, V. Subrahmanian and O. Udrea, "Machine recognition of human activities: A survey," IEEE Trans. Circuits Syst. Video Technology, vol.18, no.11, pp.1473-1488, 2008.

[70] GS1 Standards, http://www.gs1.org/epc-rfid.

[71] L.G. Robert, "Aloha packet system with and without slots and capture," ACM SIGCOMM Comput. Commun. Rev., vol.5, no.2, pp.28-42, 1975.

[72] R.D. Yates and D.J. Goodman, Probability and Stochastic Processes, 2nd Edition, John Wiley & Sons, Inc., pp.257-269, 2005.

[73] I.D. Dinov, N. Christou, and J. Sanchez, "Central limit theorem: New

SOCR applet and demonstration activity," Journal of Statistics Education, vol.16, no. 2, pp.1-15, 2008.

[74] G.D. Forney, Jr., "The Viterbi algorithm," Proceedings of the IEEE 61(3) pp. 268–278, 1973.

[75] B. W. Matthews, "Comparison of the predicted and observed secondary structure of T4 phage lysozyme," Biochimica et Biophysica Acta (BBA) - Protein Structure. pp. 442–451, 1975.

[76] G. Jurman, S. Riccadonna, and C. Furlanello, "A comparison of MCC and CEN error meaures in multi-class prediction," PLos ONE, vol.7, no.8, 2012.

[77] "CONFIDEX", online at http://www.confidex.com/.

[78] D. Kim, M. A. Ingram, and W. W. Smith, "Measurements of small-scale fading and path loss for long range RF tags," IEEE Transactions on Antennas and Propagation, vol. 51, no. 8, pp. 1740-1749, Nov. 2003.

[79] L. W. Mayer, M. Wrulich, and S Caban, "Measurements and channel modeling for short range indoor UHF applications," Proceedings of The European Conference on Antennas and Propagation, 2006.

[80] Y. H. Lee and I. Marsic, "Object Motion Detection System using Passive UHF RFID Technology for a Trauma Bay," IJSTR, Volume 6–Issue 3, ISSN 2277-8616, March 2017.

[81] Y. H. Lee and I. Marsic, "A Sensing Platform for a UHF RFID System," IJSTR, Volume 6–Issue 2, ISSN 2277-8616, February 2017.